Calculated polarizabilities of BaF, SrF and CaF using the relativistic finite-field Fock-Space Coupled Cluster method.

J. M. de Wit
Supervisors: dr. A. Borschevsky and prof. dr. S. Hoekstra

August 2018

In this thesis, the results of the parallel and perpendicular polarizability calculations on the ground state $X^2\Sigma$ and five first excited states $^2\Delta_{3/2}$, $^2\Delta_{5/2}$, $^2\Pi_{1/2}$, $^2\Pi_{3/2}$ and $B^2\Sigma$ of barium monofluoride (BaF), strontium monofluoride (SrF) and calcium monofluoride (CaF) are presented. The calculations are done using the finite-field Fock-Space Coupled Cluster method in combination with a relativistic Hamiltonian and large basis sets. The differences in polarizability of the different states and different molecules are discussed using relativity and geometry arguments. Also, results of calculations on lighter molecules magnesium monohydride (MgH) and lithium monohydride (LiH) and atoms barium (Ba), cesium (Cs) and rubidium (Rb) are presented and compared to experiment (where available) to test the accuracy of the method. Effects of using different methods, basis sets, diffuse functions, relativity and two and four component Hamiltonians is discussed.

Acknowledgements

My gratitude goes out to my supervisors Anastasia Borschevsky and Steven Hoekstra. They have taught me a lot and always had time to help, making this project a pleasurable collaboration.

I would also like to thank Pi Haase for helping me finding a way through the computational details and Yongliang Hao for sharing some of his results with me.

Contents

1 Introduction **4**
1.1 Ultracold molecules . . . 4
1.2 Search for electric dipole moment of the electron . . . 4
1.3 This work . . . 6

2 Theory **8**
2.1 Finite-field method . . . 8
2.2 Born-Oppenheimer approximation . . . 10
2.3 Relativistic Hamiltonian . . . 11
2.4 Slater determinant . . . 12
2.5 Variation principle . . . 13

3 Computational methods **15**
3.1 Dirac-Hartree-Fock method . . . 15
3.2 Coupled Cluster method . . . 17
3.3 Fock-Space Coupled Cluster method . . . 18
3.4 Basis sets . . . 20
3.5 Execution of calculations . . . 21

4 Testing of Fock-Space Coupled Cluster method **22**
4.1 Ba . . . 22
4.2 Cs . . . 23
4.3 MgH . . . 24
4.4 Rb . . . 25
4.5 LiH . . . 26

5 Results **28**
5.1 CaF . . . 29
5.1.1 Parallel component . . . 29
5.1.2 Perpendicular component . . . 33
5.2 SrF . . . 34
5.2.1 Parallel component . . . 35
5.2.2 Perpendicular component . . . 37
5.3 BaF . . . 38
5.3.1 Parallel component . . . 39
5.3.2 Perpendicular component . . . 41

6 Discussion **43**

7 Conclusion **47**

8 Appendix **51**

1 Introduction

In the field of computational chemistry, *ab initio* relativistic quantum chemistry methods are used to calculate all sorts of properties of atoms and molecules. An example of such a property is the polarizability. Using these quantum chemistry methods, the polarizability of the ground and excited states of a molecule can be determined with high accuracy. Knowledge of this property is needed in experiments involving laser-cooling and -trapping of molecules, to form ultracold molecular systems.

1.1 Ultracold molecules

Ultracold molecules are interesting systems for physicists to study, as they possess unique properties. They can be used in quantum computing and in precision measurements [1], offering promising prospects in experimental and theoretical physics. In order to perform measurements on these molecules, they need to be trapped. One way to do this is by using a light field. When in a light field, the energy levels of the molecule are shifted. This is called the ac Stark shift and this shift is proportional to the dynamical (electric) polarizability (or frequency-dependent polarizability) of the molecule. The dynamical polarizability depends on the frequency and polarization of the light. Therefore, the difference in energy of two levels depends on the light that is used to trap the molecule [2]. The frequency of the light can be chosen in such a way that the ac Stark shift is the same for the ground state and one excited state of the molecule. This is called the magic frequency. Using this magic frequency for the trapping light, the optical transition between the two energy levels of the molecule is not affected by the light [1]. This makes it possible to cool the sample further while it's still in the trap [3], creating ultracold molecules.

If light is used with a frequency that will not excite the molecule into a higher state, the dynamical polarizability can be approximated by the static polarizability, which from now on will be referred to as the polarizability. Knowledge of the polarizability is thus needed in order to successfully create ultracold molecular systems.

1.2 Search for electric dipole moment of the electron

Measuring the electric dipole moment of the electron (eEDM) is an example of a precision measurement involving ultracold molecules. Physicists have been trying to do this for quite a while and if they succeed, it could have very interesting implications in cosmology, as it could among others explain the asymmetry in matter and antimatter in our universe [4].

From the Big Bang an equal amount of matter and antimatter is expected, as each particle would be created together with its corresponding antiparticle. If particles and antiparticles would interact similarly, they would all annihilate and we would end up with a universe made out of radiation only. Instead, the universe is made mostly out of matter, with only a small fraction of antimatter. An explanation of this asymmetry could be charge conjugation parity violation, or CP violation. CP violation implies that particles and antiparticles interact in a slightly different way, leading to an asymmetry [4].

The EDM is a measure of how the electric charge is distributed. A non-zero eEDM would imply time reversal violation, or T violation. This can be explained using figure 1. A particle is depicted with a spin angular momentum in a certain direction (indicated by the black circumferential arrow), magnetic dipole moment μ (red arrow) and EDM d (purple arrow). Under T reversal, the spin will keep the same orientation with respect to the magnetic dipole moment. However, the orientation of the EDM changes with respect to the magnetic dipole moment. For a non-zero EDM, the state of the particle before time reversal is thus different from the state after time reversal, implying T violation.

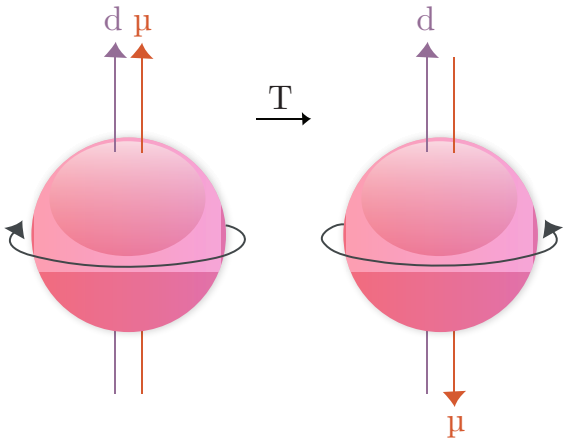

Figure 1: T violation of electron with non-zero EDM.

The CPT theorem states that the combined operation of C, P and T is a symmetry, i.e. it leaves the system invariant. Therefore, if one of the symmetries is violated, the remaining other two combined should also be violated in order to preserve CPT symmetry. Therefore, a non-zero eEDM which suggests T violation, also suggests CP violation. [5]

The Standard Model predicts the eEDM to be $d_e = \mathcal{O}(10^{-38})$ e·cm [6], which is experimentally still out of reach. Together with the other CP violating processes in the Standard Model, this predicted eEDM is too small to account for enough CP violation to explain the matter-antimatter asymmetry in the universe. This could mean that physics beyond the Standard Model is needed to account for extra CP violation. Including new particles in the model can give rise to a much larger eEDM, which could be measured experimentally. The NL-eEDM collaboration is a collaboration of scientists from The Netherlands (Nikhef, University of Groningen, Vrije Universiteit) which aims to improve the measurement of the eEDM [7]. In their experiment they will be using cold BaF molecules, aiming for a sensitivity of $5 \cdot 10^{-30}$ e·cm. In figure 2, some experimental eEDM upper limits of previous experiments are shown, together with the aim of the NL-eEDM collaboration (referred to by 'This program'). The measurement of the eEDM serves as a probe into beyond Standard Model physics.

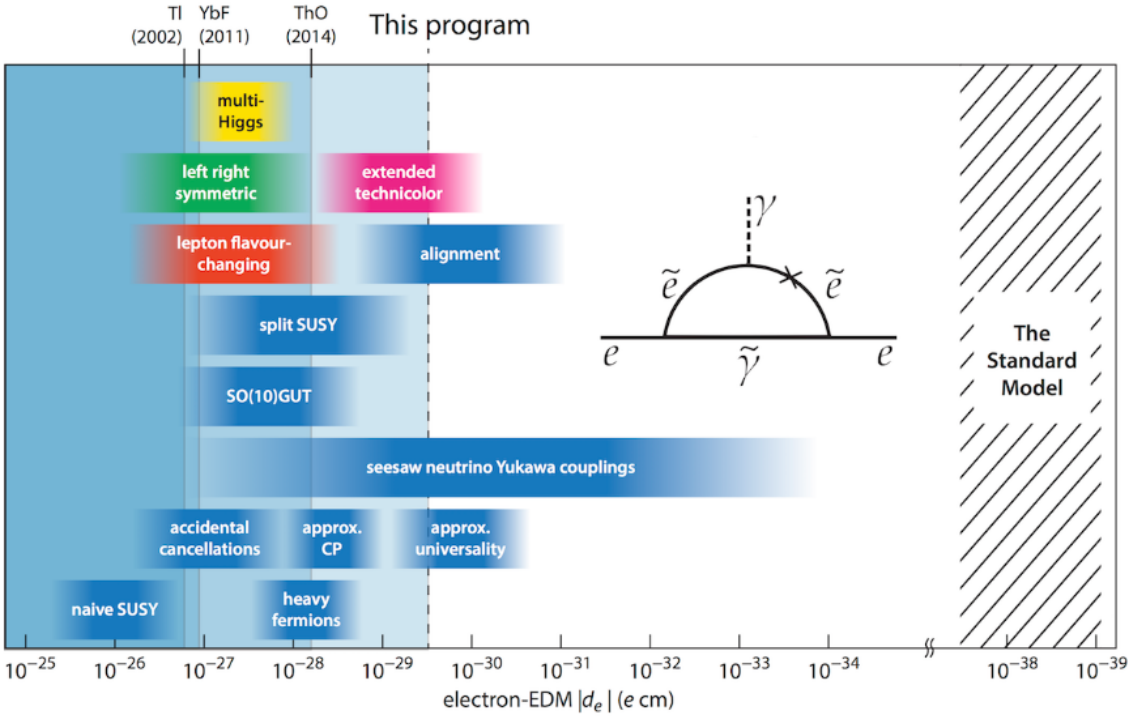

Figure 2: The experimental upper limits of the eEDM and their impact on extensions of the Standard Model. [7]

BaF is used in this experiment because it is a heavy paramagnetic diatomic molecule with a relative large effective electric field E_{eff}. This field can be interpreted as the net electric field felt by an electron in the molecule. It can't be measured experimentally, but it can be calculated as well by using *ab initio* relativistic quantum chemistry methods. The interaction between an electron and E_{eff} results in a linear Stark shift $\Delta E \propto d_e E_{\text{eff}}$ [8], which is what actually will be measured in the experiment. From this a limit for the eEDM can be extracted.

1.3 This work

As knowledge about the polarizability of BaF is needed to create a system of ultracold BaF, it was calculated together with the polarizabilities of the similar but lighter molecules SrF and CaF and the results are presented in this thesis. The lighter molecules are also of interest, as they can be used in experiments involving laser trapping as well.

The calculations are performed using the *ab initio* Dirac-Hartree-Fock method in combination with the finite-field Fock-Space Coupled Cluster method. Also, some calculations are done using the single-reference Coupled Cluster method. A relativistic Hamiltonian is used, because relativistic effects can't be neglected in these heavy molecules. In the methods, the wavefunction of the molecules are represented by functions from a basis set. The aim in this research is to add mas many functions to the basis set as possible until convergence is reached, i.e. the results do not change when adding more functions. In this way, the best possible result is obtained in this computational framework.

In order to get to know the Fock-Space Coupled Cluster method, calculations are first done on the lighter atoms and molecules MgH, LiH, Ba, Cs and Rb. For some of these systems experimental values of the polarizability are available, in contrast to BaF, SrF and CaF. By comparing the calculated values to these experimental values, the effect of using different methods, Hamiltonians and basis sets is tested.

2 Theory

The definition of the polarizability is as follows:

***Polarizability**: the tendency of the electron cloud of a molecule or atom to get distorted by an external electric field.*

The polarizability can be described using the finite-field method, where the energy of the molecule is evaluated in different external electric fields. The polarizability is extracted numerically from the derivative of the energy with respect to the field.

2.1 Finite-field method

When in an external electric field, the energy levels of an atom or molecule will shift, known as the Stark shift. The dependence of the particle's energy ε on an external static electric field E can be written as a Taylor expansion around zero [9]:

$$\begin{aligned} \varepsilon(E) &= \varepsilon(0) + \frac{\partial \varepsilon}{\partial E}\Big|_0 E + \frac{1}{2!}\frac{\partial^2 \varepsilon}{\partial E^2}\Big|_0 E^2 \dots \\ &\equiv \varepsilon(0) - \mu E - \frac{1}{2}\alpha E^2 \cdots \end{aligned} \tag{1}$$

Here, μ is the permanent dipole moment of the particle and α is the polarizability. If very small fields are used, the higher order terms can be neglected.

The Stark shift is thus, approximately:

$$\Delta\varepsilon = \mu E - \frac{1}{2}\alpha E^2 \tag{2}$$

For diatomic molecules, two components of the polarizability can be defined: perpendicular and parallel to the internuclear axis, which is chosen to be along the z-axis (see figure 3). Because of the symmetry of the molecule, the component in the x direction is the same as in the y direction.

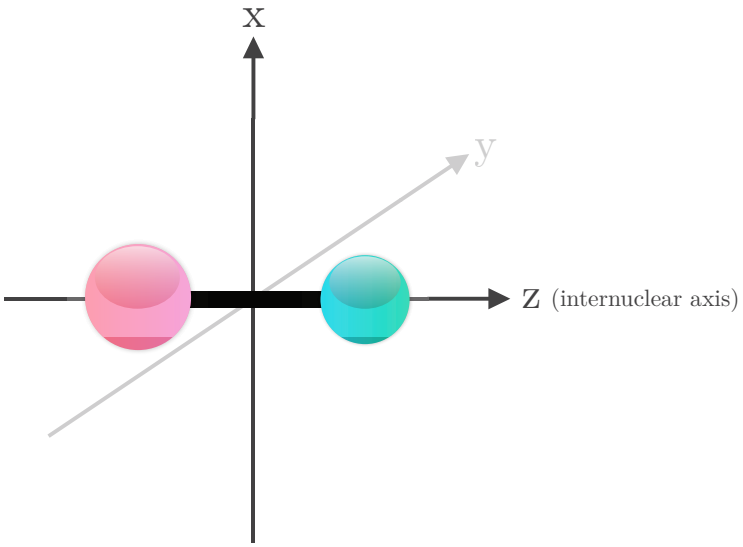

Figure 3: Schematic picture of diatomic molecule.

To get the parallel component, the external electric field is pointed along the internuclear axis to get:

$$\Delta\varepsilon_z = -\mu E_z - \frac{1}{2}\alpha_z E_z^2 \tag{3}$$

Where α_z is the parallel component of the polarizability.

Directing the electric field perpendicular to the internuclear axis will give the perpendicular component of the polarizability. As the permanent dipole moment is directed along the internuclear axis, the first term is zero:

$$\Delta\varepsilon_x = -\frac{1}{2}\alpha_x E_x^2 \tag{4}$$

Where α_x is the perpendicular component of the polarizability. This is also the Stark shift in an atom, since atoms do not possess a permanent dipole moment.

Equation 3 still holds a dependence on the permanent dipole moment of the molecule, which is unknown in some cases. To get rid of the first term, the Stark shift of an electric field E_z is added to the Stark shift of a negative electric field with the same magnitude $-E_z$. The first term will cancel:

$$\begin{aligned}\Delta\varepsilon_{E_z} + \Delta\varepsilon_{-E_z} &= \Big[-\mu E_z - \frac{1}{2}\alpha_z E_z^2\Big] + \Big[-\mu(-E_z) - \frac{1}{2}\alpha_z(-E_z)^2\Big] \\ &= -\mu E_z - \frac{1}{2}\alpha_z E_z^2 + \mu E_z - \frac{1}{2}\alpha_z E_z^2 \\ &= -\alpha_z E_z^2\end{aligned} \tag{5}$$

In this way, no knowledge about the permanent dipole moment is required.

In order to calculate the polarizability, the energy shifts caused by three different external electric

fields are calculated and the polarizability is then extracted numerically. The energy shifts are calculated using the Dirac-Hartree-Fock, single-reference Coupled Cluster and Fock-Space Coupled Cluster method, which all involve solving some altered version of the time-independent Schrödinger equation:

$$\hat{H}|\Psi\rangle = E|\Psi\rangle \tag{6}$$

As solving this equation for systems heavier than hydrogen is not possible, some appropriate approximation of the Hamiltonian $\hat{H}$ and wavefunction $|\Psi\rangle$ of the system is needed. As the molecules considered in this thesis are heavy molecules, a relativistic Hamiltonian is used. Also, the Born-Oppenheimer approximation is invoked and the wavefunction is approximated by a Slater determinant. These matters will be discussed in the following sections, before moving on to the explanation of the computational methods.

2.2 Born-Oppenheimer approximation

Since nuclei are very heavy relative to electrons, the former can be considered as being static with respect to the electrons. This is called the Born-Oppenheimer approximation and it will make it a lot easier to deal with the Schrödinger equation. A certain geometry can be selected for the nuclei and the motion of the electrons relative to the nuclei can be considered. In this way, the wavefunction can be written as a product of an electronic and nuclear component:

$$|\Psi_{\text{total}}\rangle = |\Psi_e\rangle|\Psi_N\rangle \tag{7}$$

The molecular Hamiltonian will have several terms depending on the positions of the nuclei and electrons:

$$\begin{aligned}\hat{H}_{\text{total}} &= -\frac{1}{2}\sum_A \frac{1}{M_A}\nabla_A^2 + \sum_{A\neq B}\frac{Z_A Z_B}{R_{AB}} - \frac{1}{2}\sum_i \nabla_i^2 - \sum_{A,i}\frac{Z_A}{r_{iA}} + \frac{1}{2}\sum_{i\neq j}\frac{1}{r_{ij}} \\ &= \left[\hat{T}_N(\mathbf{R}) + \hat{V}_{NN}(\mathbf{R})\right] + \left[\hat{T}_e(\mathbf{r}) + \hat{V}_{eN}(\mathbf{r},\mathbf{R}) + \hat{V}_{ee}(\mathbf{r})\right] \\ &\equiv \hat{H}_N + \hat{H}_e\end{aligned} \tag{8}$$

Here, $\hat{T}_N$ is the nuclear kinetic energy term, $\hat{T}_e$ is the electronic kinetic energy term, $\hat{V}_{NN}$ is the nuclear-nuclear repulsion, $\hat{V}_{ee}$ is the electron-electron repulsion and $\hat{V}_{eN}$ is the electron-nuclear attraction.

The Schrödinger equation can now be written as:

$$\hat{H}_{\text{total}}|\Psi_{\text{total}}\rangle = \left(\hat{H}_N + \hat{H}_e\right)|\Psi_e\rangle|\Psi_N\rangle \tag{9}$$

The electronic part can be solved first for specific nuclear coordinates ($\mathbf{R}$) and then the obtained energy can be used to solve the total Schrödinger equation [10].

The potential between nuclei and electrons ($\hat{V}_{eN}$) will then only depend on the coordinates of the nuclei $\mathbf{R}$ parametrically.

$$\begin{aligned}\hat{H}_e|\Psi_e\rangle &= \left[\hat{T}_e(\mathbf{r}) + \hat{V}_{eN}(\mathbf{r};\mathbf{R}) + \hat{V}_{ee}(\mathbf{r})\right]|\Psi_e\rangle \\ &= E_e|\Psi_e\rangle\end{aligned} \tag{10}$$

This is the electronic Schrödinger equation.

It can be shown that [10]:

$$\begin{aligned} \hat{T}_e|\Psi_e\rangle|\Psi_N\rangle &= |\Psi_N\rangle\hat{T}_e|\Psi_e\rangle \\ \hat{T}_N|\Psi_e\rangle|\Psi_N\rangle &= |\Psi_e\rangle\hat{T}_N|\Psi_N\rangle \end{aligned} \tag{11}$$

Using this, equation 9 can be reformulated like (omitting the arguments of the operators) :

$$\begin{aligned} \hat{H}_{\text{total}}|\Psi_{\text{total}}\rangle &= |\Psi_N\rangle\Big(\hat{T}_e + \hat{V}_{eN} + \hat{V}_{ee}\Big)|\Psi_e\rangle + \Big(\hat{T}_N + \hat{V}_{NN}\Big)|\Psi_e\rangle|\Psi_N\rangle \\ &= |\Psi_N\rangle E_e|\Psi_e\rangle + \Big(\hat{T}_N + \hat{V}_{NN}\Big)|\Psi_e\rangle|\Psi_N\rangle \\ &= \Big(E_e + \hat{T}_N + \hat{V}_{NN}\Big)|\Psi_e\rangle|\Psi_N\rangle \\ &= E_{\text{total}}|\Psi_{\text{total}}\rangle \end{aligned} \tag{12}$$

Which leaves us with:

$$\Big(E_e + \hat{T}_N + \hat{V}_{NN}\Big)|\Psi_N\rangle = E_{\text{total}}|\Psi_N\rangle \tag{13}$$

Hence, the energy obtained from the electronic Schrödinger equation is used in this last equation to obtain the total energy.

2.3 Relativistic Hamiltonian

When dealing with heavy molecules, relativistic effects can't be neglected. The electrons feel a large attractive force from the heavy nucleus, accelerating them to speeds close to the speed of light. A consequence of this is the contraction of the s- and p$\frac{1}{2}$-shells, causing them to be stronger bound and energetically stabilized. As a direct result of that, the d- and f-shells feel less attraction from the nucleus, making them energetically destabilized [11].

Relativistic effects are taken into account by using for the electronic Hamiltonian the four component relativistic Dirac-Coulomb Hamiltonian in the calculations [12]:

$$H_{DC} = \sum_i h_D(i) + \frac{1}{2}\sum_{i\neq j}\frac{1}{r_{ij}} \tag{14}$$

And h_D is the one-electron Dirac Hamiltonian:

$$h_D = c\boldsymbol{\alpha}\cdot\mathbf{p} + \beta c^2 + V_{nuc} \tag{15}$$

Where $\boldsymbol{\alpha}$ and β are the four-component Dirac matrices, $\mathbf{p}$ is the four-momentum of the electron and V_{nuc} is the nuclear potential.

The Dirac wavefunction is a four component vector:

$$\Psi_{4c} = \begin{pmatrix} \Psi^L \\ \Psi^S \end{pmatrix} \tag{16}$$

Where Ψ^L and Ψ^S are two component functions, corresponding to positive energy E^+ (electronic) states and negative energy E^- (positronic) states, respectively [13].

The two component wavefunctions are related by [13]:

$$\begin{aligned} \Psi^S &= R\Psi^L \\ R &= \frac{c(\sigma \cdot \mathbf{p})}{2mc^2 - V_{nuc} + E^+} \end{aligned} \tag{17}$$

Where σ represents the Pauli spin matrices. R can be used to express the four component wavefunction Ψ_{4c} in terms of Ψ^L. This results (after some manipulations) in a two component wavefunction:

$$\Psi^+_{2c} = \sqrt{1 + R^\dagger R}\Psi^L \tag{18}$$

Here, $R^\dagger$ is the hermitian conjugate of R.

With the help of R, a two component Hamiltonian can be defined as well, known as the X2C Hamiltonian [14]. It will reproduce the positive energy spectrum of the four component Hamiltonian h_D [13]. In general, using the X2C Hamiltonian will give somewhat different results, as Ψ^S is left out. However, the full relativistic results are very well approximated by the two component approach (as is shown later). As the two component approach requires less computational resources, it's a good alternative to the four component approach.

2.4 Slater determinant

Each electron of the atom or molecule can be described by a single-particle wavefunction χ, called an orbital. These orbitals are all independent of each other, and they move in an average potential caused by the other electrons. The simplest case would be a system containing only one electron. If another electron would be added to the system, the orbitals of the two electrons can in principle be multiplied, giving the total wavefunction:

$$\Psi_e(\mathbf{x_1}, \mathbf{x_2}) = \chi_1(\mathbf{x_1})\chi_2(\mathbf{x_2}) \tag{19}$$

Where $\mathbf{x_1}$ and $\mathbf{x_2}$ are the four vectors which describe the spatial and spin state of the electrons. Electrons are fermions, meaning that they must obey the Pauli exclusion principle: electrons can't be in the same quantum state simultaneously. The total wavefunction must be antisymmetric, meaning that it changes sign when the spatial and spin states of two electrons are interchanged. This is clearly not the case for the wavefunction in equation 19, meaning that this is not a proper way to describe the system. Consider the following wavefunction [15]:

$$\Psi_e(\mathbf{x_1}, \mathbf{x_2}) = \frac{1}{\sqrt{2}}[\chi_1(\mathbf{x_1})\chi_2(\mathbf{x_2}) - \chi_1(\mathbf{x_2})\chi_2(\mathbf{x_1})] \tag{20}$$

This wavefunction is indeed antisymmetric under the interchange of the spatial and spin states. This wavefunction can be extended from two to n electrons using the following determinant, called the

Slater determinant [15]:

$$\Psi_e(\mathbf{x_1}...\mathbf{x}_n) = \frac{1}{\sqrt{n!}} \begin{vmatrix} \chi_1(\mathbf{x_1}) & \chi_2(\mathbf{x_1}) & \dots & \chi_n(\mathbf{x_1}) \\ \chi_1(\mathbf{x_2}) & \chi_2(\mathbf{x_2}) & \dots & \chi_n(\mathbf{x_2}) \\ \vdots & \vdots & \ddots & \vdots \\ \chi_1(\mathbf{x}_n) & \chi_2(\mathbf{x}_n) & \dots & \chi_n(\mathbf{x}_n) \end{vmatrix} \tag{21}$$

This wavefunction is used in the Dirac-Hartree-Fock method as an approximation to the actual wavefunction.

2.5 Variation principle

Another useful tool employed is the variation principle [16], which states that the energy corresponding to any trail function will always be higher than the actual ground state energy. This can be proven in the following way:

The trial wavefunction may be expressed as a linear combination of the actual (normalized) eigenfunctions ψ_i of the Hamiltonian:

$$\Psi_{\text{trial}} = \sum_i c_i \psi_i \tag{22}$$

If the trail wavefunction is normalized as well, it can be shown that:

$$\begin{aligned} 1 &= \langle \Psi_{\text{trial}} | \Psi_{\text{trial}} \rangle \\ &= \big\langle \sum_i c_i \psi_i \big| \sum_j c_j \psi_j \big\rangle \\ &= \sum_{i,j} c_i^* c_j \langle \psi_i | \psi_j \rangle \\ &= \sum_{i,j} c_i^* c_j \delta_{ij} \\ &= \sum_i |c_i|^2 \end{aligned} \tag{23}$$

The energy corresponding to the trail wavefunction would be:

$$\begin{aligned} \langle \Psi_{\text{trial}} | H | \Psi_{\text{trial}} \rangle &= \big\langle \sum_i c_i \psi_i \big| H \big| \sum_j c_j \psi_j \big\rangle \\ &= \sum_{i,j} \langle c_i \psi_i | E_j | c_j \psi_j \rangle \\ &= \sum_i |c_i|^2 E_i \end{aligned} \tag{24}$$

Per definition, the ground state wavefunction always corresponds to the lowest energy possible, so $E_i \geq E_g$ for all i, where E_g is the ground state energy.

Therefore:

$$\langle \Psi_{\text{trial}} | H | \Psi_{\text{trial}} \rangle = \sum_i |c_i|^2 E_i \geq E_g \sum_i |c_i|^2 = E_g \tag{25}$$

So, when using a trial wavefunction, the calculated energy will always be an upper bound. This principle is used in the Dirac-Hartree-Fock method, explained in the following section.

3 Computational methods

The Dirac-Hartree-Fock method will give an estimation of the energy and wavefunction of an atom or molecule. This method alone will not be sufficient, as it neglects explicit interactions between electrons. For that, another method will be used, which in this case will be the Fock-Space Coupled Cluster method. This is a multi-reference method, meaning that it will give information on the ground state and excited states in one run. Also, the single-reference Coupled Cluster method will be used in some preparatory work. The basics of these methods will be explained in this section.

3.1 Dirac-Hartree-Fock method

The Dirac-Hartree-Fock method (DHF) is designed to solve the electronic Schrödinger equation, within the Born-Oppenheimer approximation. It starts with a trial wavefunction, described by a Slater determinant. According to the variation principle, this will give a higher energy than the actual ground state energy. To get the wavefunction with the greatest resemblance to the exact wavefunction, the trial wavefunction is varied iteratively until a minimum in energy is reached. So, the following equation needs to be minimized [15]:

$$E_e = \langle \Psi | \hat{H}_e | \Psi \rangle \tag{26}$$

This equation can be written in terms of one- and two-electron operators, giving the Hartree-Fock energy [15]:

$$E_{\mathrm{HF}} = \sum_i \langle i|h|j\rangle + \frac{1}{2}\sum_{ij}[ii|jj] - [ij|ji] \tag{27}$$

Where the first term is the one-electron integral:

$$\langle i|h|j\rangle = \int d\mathbf{x_1}\chi_i^*(\mathbf{x_1})h(\mathbf{r_1})\chi_j(\mathbf{x_1}) \tag{28}$$

And the second term is the two-electron integral:

$$[ij|kl] = \int d\mathbf{x_1}d\mathbf{x_2}\chi_i^*(\mathbf{x_1})\chi_j(\mathbf{x_1})\frac{1}{r_{12}}\chi_k^*(\mathbf{x_2})\chi_l(\mathbf{x_2}) \tag{29}$$

The Hartree-Fock energy equation needs to be minimized with respect to small changes in the orbitals $\chi_i \rightarrow \chi_i + \delta\chi_i$. It's assumed that the orbitals χ are orthonormal, and in order to keep them orthonormal during the procedure of variation, Langrange method of undetermined mulitpliers is employed, using the following experssion [15]:

$$\mathcal{L}[\{\chi_i\}] = E_{HF}[\{\chi_i\}] - \sum_{ij}(\langle i|j\rangle - \delta_{ij}) \tag{30}$$

Where $\langle i|j\rangle$ is the overlap between the spin orbitals j and i. After some algebra, one arrives at the Hartree-Fock equation [15]:

$$h(\mathbf{x_1})\chi_i(\mathbf{x_1}) + \sum_{j\neq i}\Big[\int d\mathbf{x_2}|\chi_j(\mathbf{x_2})|^2\frac{1}{r_{12}}\Big]\chi_i(\mathbf{x_1}) - \sum_{j\neq i}\Big[\int d\mathbf{x_2}\chi_j^*(\mathbf{x_2})\chi_i(\mathbf{x_2})\frac{1}{r_{12}}\Big]\chi_j(\mathbf{x_1}) = \epsilon_i\chi_i(\mathbf{x_1}) \tag{31}$$

Here, ϵ_i is the energy eigenvalue corresponding to χ_i.

The first sum in equation 31 is known as the Coulomb term and it represents the interaction of orbital χ_i with the average potential arising from the other orbitals. The term in brackets is referred to by $\mathcal{J}_j(\mathbf{x_1})$.

The second sum arises from the requirement of the wavefunction to be antisymmetrical, known as the exchange term. The term in brackets is referred to by $\mathcal{K}_j(\mathbf{x_1})\chi_i(\mathbf{x_1})\chi_j^*(\mathbf{x_1})$. With this new notation, equation 31 simplifies to:

$$\Big[h(\mathbf{x_1}) + \sum_j \mathcal{J}_j(\mathbf{x_1}) - \mathcal{K}_j(\mathbf{x_1})\Big]\chi_i(\mathbf{x_1}) = \epsilon_i\chi_i(\mathbf{x_1}) \tag{32}$$

The term between brackets is knows as the Fock operator $f(\mathbf{x_1})$, giving the simplified Hartree-Fock equation:

$$f(\mathbf{x_1})\chi_i(\mathbf{x_1}) = \epsilon_i\chi_i(\mathbf{x_1}) \tag{33}$$

To solve this equation, a description of the orbitals χ is required. Mathematically this is done by taking linear combinations of basis functions, obtained from a basis set (see section 'Basis sets'). If the basis functions are denoted by $\tilde{\chi}$, the orbitals χ can be expressed in terms of the basis functions like [15]:

$$\chi_i = \sum_{\mu=1}^{K} C_{\mu i}\tilde{\chi_\mu} \tag{34}$$

Where K is the number of basis functions in the basis set. When placed in the Hartree-Fock equation, multiplying from the left with $\tilde{\chi}_i^*(\mathbf{x_1})$ and integrating, the following is obtained:

$$\sum_\nu F_{\nu\mu}C_{\nu i} = \epsilon_i \sum_\nu S_{\mu\nu}C_{\nu i} \tag{35}$$

Where, $F_{\mu\nu}$ and $S_{\mu\nu}$ are the matrix elements [15]:

$$F_{\mu\nu} = \int d\mathbf{x_1}\tilde{\chi}_\mu^*(\mathbf{x_1})f(\mathbf{x_1})\tilde{\chi}_\nu(\mathbf{x_1}) \tag{36}$$

$$S_{\mu\nu} = \int d\mathbf{x_1}\tilde{\chi}_\mu^*(\mathbf{x_1})\tilde{\chi}_\nu(\mathbf{x_1}) \tag{37}$$

Equations 35 can be written in the simple matrix form like:

$$FC = \epsilon SC \tag{38}$$

This equation is known as the Hartree-Fock-Roothaan equation [15]. By performing matrix transformations, this equation is solved in each iteration of the Dirac-Hartree-Fock method. The optimized wavefunction resulting from this method will be used in the Fock-Space Coupled Cluster or single reference Coupled Cluster method. It will be referred to as $|\Psi_{\mathrm{HF}}\rangle$.

3.2 Coupled Cluster method

As mentioned before, in the Dirac-Hartree-Fock method the electrons are assumed to be independent of each other. They move in an average potential caused by the other electrons. In reality this is not the case, making this method a crude estimation. Instantaneous interaction between electrons (electron correlation) needs to be included in the calculations, as electron correlation will lower the energy due to the reduction of electron-electron repulsion. One way to do this is by using the Coupled Cluster method [17].

As electrons repel each other, it might happen that an electron will be excited to a higher energy level in order to avoid an other electron. This is called a single excitation. This can be described by an excitation operator acting on the wavefunction obtained in the Dirac-Hartree-Fock method: $\hat{T}_1|\Psi_{\text{HF}}\rangle$. Sometimes two electrons get excited: a double excitation, as illustrated in figure 4b. This process can be described by an operator $\hat{T}_2$ acting on the wavefunction: $\hat{T}_2|\Psi_{\text{HF}}\rangle$.

Another possibility is that two pairs of electrons are exited independently, as in figure 4c . This is described by applying the operator twice: $\frac{1}{2}T_2^2|\hat{\Psi}_{\text{HF}}\rangle$, with a multiplication of $\frac{1}{2}$ to avoid double counting the pairs. Generalizing to m excited pairs this will give: $\frac{1}{m!}\hat{T}_2^m|\Psi_{\text{HF}}\rangle$. As m can be any number, a summation over m is required. This can be written as the series expansion of e^x:

$$\sum_{m=0}^{\infty}\frac{1}{m!}\hat{T}_2^m|\Psi_{\text{HF}}\rangle = e^{\hat{T}_2}|\Psi_{\text{HF}}\rangle \tag{39}$$

As can be seen in figure 4d, a similar thing can happen for three electrons. This is called triple excitation and it can be described in a similar way as double excitation. For n independent triple excitations we get $\frac{1}{n!}\hat{T}_3^n|\Psi_{\text{HF}}\rangle$. Double and triple excitation can also happen at the same time, which will look like $\frac{1}{m!n!}\hat{T}_2^m T_3^n|\Psi_{\text{HF}}\rangle$. When we sum over n and m, we get $e^{\hat{T}_2+\hat{T}_3}|\Psi_{\text{HF}}\rangle$. Generalized for a total number of electrons N, we get:

$$e^{\hat{T}_1+\hat{T}_2+\hat{T}_3+\hat{T}_4+\ldots+\hat{T}_N}|\Psi_{\text{HF}}\rangle = e^{\hat{\mathbf{T}}}|\Psi_{\text{HF}}\rangle \tag{40}$$

The excitation operators can be written in a second-quantization formalism. $\hat{T}_1$ and $\hat{T}_2$ have the following form

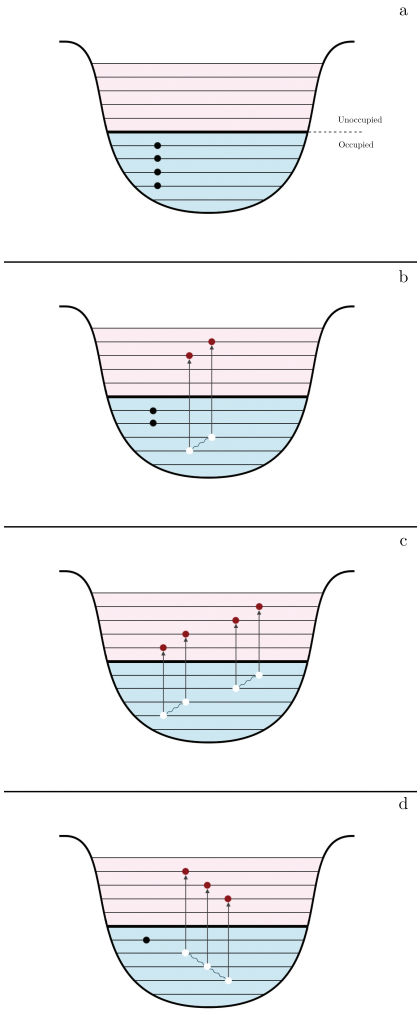

Figure 4: Electron correlation (based on a picture from [17]).

[18]:

$$\hat{T}_1 = \sum_{a}^{occ} \sum_{i}^{virt} t_a^i \hat{a}_i^\dagger \hat{a}_a \tag{41}$$

$$\hat{T}_2 = \frac{1}{4} \sum_{a,b}^{occ} \sum_{i,j}^{virt} t_{ab}^{ij} \hat{a}_i^\dagger \hat{a}_j^\dagger \hat{a}_b \hat{a}_a \tag{42}$$

Here, t_{ab}^{ij} are the cluster amplitudes that need to be determined and $\hat{a}_i^\dagger$ and $\hat{a}_a$ are the creation and annihilation operators, respectively.

Usually, the calculation is truncated at $\hat{T}_2$, only including single and double excitations (CCSD). It's also common to include triple excitations pertubatively (CCSD(T)), giving even better results.

The energy can be calculated using [19]:

$$E = \langle \Psi_{\mathrm{HF}} | \hat{H} e^{\hat{\mathbf{T}}} | \Psi_{\mathrm{HF}} \rangle \tag{43}$$

And the amplitudes are determined using the equation [19]:

$$\langle \mu_i | e^{-\hat{\mathbf{T}}} H e^{\hat{\mathbf{T}}} | \Psi_{\mathrm{HF}} \rangle = 0 \tag{44}$$

Where $\langle \mu_i | = \langle \Psi_{\mathrm{HF}} | \hat{a}_i^\dagger$.

The Coupled Cluster method is also known as the single-reference Coupled Cluster method. It can already be deduced from the name: this is a method relying on a single reference state, which would be the state obtained from the Dirac-Hartree-Fock method $|\Psi_{\mathrm{HF}}\rangle$. In some cases, a multi-reference method, such as Fock-Space Coupled Cluster can be more convenient. This method will be discussed in the following section.

3.3 Fock-Space Coupled Cluster method

The Fock-Space Coupled Cluster (FSCC) method [20] starts with a reference or vacuum state, which has to be a closed shell state. This corresponds to an ion of the system of interest and the wavefunction of this ion is obtained in the Dirac-Hartree-Fock calculation. Different sectors are defined, where sector (m, n) includes all the states where m electrons are removed and n electrons are added to the vacuum state. The model space P comprises the orbitals where the electrons are allowed to sit.

Let's consider an example. Neutral carbon has the ground state $1s^2 2s^2 2p^2$. The first two s-shells hold the core orbitals, as they are closed. The p-shell hold the valence orbitals and higher shells will hold virtual orbitals. The vacuum state would be $1s^2 2s^2$ and to get information about the ground state (and some excited states), sector $(0, 2)$ is needed, as it comprises all states with two electrons added in the p-shell. The model space can be chosen to be the p-orbitals, but other virtual orbitals can be included as well.

Including a number of different states in the model space is what makes this method a multi-reference

method. Single-reference methods generally give very accurate results for systems that are described well by a single Slater determinant such as closed-shell systems, but for open-shell systems it can fail. For example, when there is another low-lying state close to the ground state. Let's say there would be a low-lying configuration $1s^2 2p^4$ in carbon. In order to get reliable results, this state needs to be included in the model space [21], which can be done only in multi-reference methods. An additional benefit of this is that energies of multiple excited states as well as the ground state is calculated at once, whereas in single-reference methods only the energy of the reference state is calculated.

The model space P is thus a set of virtual orbitals $\{|\psi_i\rangle\}$. This model space is the starting point for getting the set $\{|\Psi_i\rangle\}$ of exact solutions of the Schrödinger equation. We define the projection operator [21]:

$$\hat{P} = \sum_i |\psi_i\rangle\langle\psi_i| \tag{45}$$

which has a orthogonal complement $\hat{Q} = 1 - \hat{P}$.

When intermediate normalization is assumed:

$$\langle\psi_i|\Psi_i\rangle = \langle\psi_i|\psi_i\rangle = 1 \tag{46}$$

$$\langle\psi_i|\Psi_j\rangle = \langle\psi_i|\psi_j\rangle = 0 \tag{47}$$

we can see that [22]:

$$|\psi_i\rangle = \hat{P}|\Psi_i\rangle \tag{48}$$

The operator $\hat{\Omega}$ establishes a reverse mapping and generates the exact wavefunction from one belonging to the model space [22]:

$$|\Psi_i\rangle = \hat{\Omega}|\psi_i\rangle \tag{49}$$

An ansatz for $\hat{\Omega}$ used in multi-reference Coupled Cluster methods is [19]:

$$\hat{\Omega} = e^{\hat{S}} = 1 + \hat{S} + \frac{1}{2}\hat{S}^2 \cdots \tag{50}$$

The operator $\hat{S}$ excites electrons from the model space P to Q. $\hat{S}$ can also be partitioned according to the different sectors [19]:

$$\hat{S} = \hat{S}^{(0,0)} + \hat{S}^{(0,1)} + \hat{S}^{(1,0)} + \hat{S}^{(1,1)} + \cdots \tag{51}$$

Where $\hat{S^{(0,0)}}$ is equal to the single-reference Coupled Cluster operator $\hat{T}$. For each sector, different terms of $\hat{S}$ are included in the calculations. In the case of the carbon example given earlier, only the terms $\hat{S}^{(0,0)}, \hat{S}^{(0,1)}$ and $\hat{S}^{(0,2)}$ are needed to obtain the ground state.

Next, the so-called FSCC equations need to be solved. This is done for each sector separately, starting with sector $(0,0)$ and using $\hat{S}^{(0,0)}$ (which is equivalent to the calculation in single-reference Coupled Cluster method). The result of this calculation is then used in the next sector calculation, and so on, reducing the computational effort. [19]

The exact Schrödinger equation $\hat{H}|\Psi_i\rangle = E_i|\Psi_i\rangle$ in combination with equation 49 may be written as:

$$\hat{H}\hat{\Omega}|\psi_i\rangle = E_i\hat{\Omega}|\psi_i\rangle \tag{52}$$

If $\hat{\Omega}$ has an inverse, i.e. $\hat{\Omega}\hat{\Omega}^{-1} = \hat{\Omega}^{-1}\hat{\Omega} = 1$, equation 52 can be multiplied by the inverse and the following is obtained [22]:

$$\hat{\Omega}^{-1}\hat{H}\hat{\Omega}|\psi_i\rangle = \hat{\Omega}^{-1}E_i\hat{\Omega}|\psi_i\rangle = E_i|\psi_i\rangle \tag{53}$$

The operator $\hat{\Omega}^{-1}\hat{H}\hat{\Omega}$ acts as a effective Hamiltonian $\hat{H}_{\text{eff}}$.

The FSCC equations are derived by placing $\hat{\Omega}$ in the Bloch equation [20]:

$$\left[\hat{\Omega}, \hat{H}_0\right]\hat{P} = \left(\hat{V}\hat{\Omega} - \hat{\Omega}\hat{H_{\text{eff}}}\right)\hat{P} \tag{54}$$

Where the Hamiltonian $\hat{H} = \hat{H}_0 + \hat{V}$ is partitioned in the usual way. This yields $\hat{H_{\text{eff}}}$. The relevant energies can now be calculated by solving:

$$\hat{H}_{\text{eff}}|\psi_i\rangle = E_i|\psi_i\rangle \tag{55}$$

This yields a number of energies, the energies of each sector, in only one calculation.

3.4 Basis sets

As mentioned in the section about the Dirac-Hartree-Fock method, the orbitals χ are mathematically described by linear combinations of basis functions. These basis functions are again linear combinations of Gaussian functions, which look like [23]:

$$g_{ijk} = Nx^i y^j z^k e^{-\alpha r^2} \tag{56}$$

Here N is a normalization constant, i, j and k are positive integers and α is a positive orbital exponent.

The minimal basis set would be the one where only one basis function is used to describe each orbital. To get a better description, more basis functions can be used to describe the valence orbitals. The number of basis sets used is indicated by the names double-zeta (two basis functions), triple-zeta (three basis functions), quadruple-zeta (four basis functions), etcetera.

A way to get the description of the wavefunction more accurate, is to add diffuse functions to the basis set. Diffuse functions have small exponents, describing a larger region of space [23]. This can be important in calculations where electrons are far away from the nucleus. This is the case for polarizability calculations, as the outer electrons are affected the most by an external electric field.

In this thesis, the relativistic Dyall basis set is used [24]. In the text they are called dyall.vxz, where x is 2, 3 or 4, which stands for the number of basis functions used. When diffuse functions are added, the basis set is called y-aug-dyall.vxz, where y can be s (single), d (double) or t (triple), the number of diffuse functions added.

3.5 Execution of calculations

All calculations were performed using the computational program DIRAC (2016 and 2017) [25]. The calculations were carried out by the Peregrine HPC cluster and Nieuwpoort cluster, both of the University of Groningen.

4 Testing of Fock-Space Coupled Cluster method

For BaF, SrF and CaF, no experimental polarizability values are availabe to which the results in this thesis can be compared. Therefore, calculations have been done on systems where experiment or other theoretical work for the polarizability is available. In this way, accuracy of the finite field FSCC method can be tested.

Calculations were performed on Ba, Cs, MgH, Rb and LiH. In the calculations, different basis sets are used to see the effect of this on the accuracy of the results. Also, the two component X2C Hamiltonian and four component Hamiltonian is used, from now on referred to by X2C and 4c. Results are presented from using the Dirac-Hartree-Fock method (DHF), single reference Coupled Cluster method including single and double excitations (CCSD) and perturbative triple excitations (CCSD(T)) and Fock-Space Coupled Cluster method (FSCC).

4.1 Ba

For Ba, the energy levels of the first four excited states were calculated and compared to experiment. Ba is a closed shell system with ground state $^1S_0$. Both sector (1,1) and sector (0,2) calculations were done, since in both sectors the vacuum state is a closed shell state. In sector (0,2) this corresponds to doubly ionized Ba. The model space was chosen to be the 6s and 6p orbitals. In sector (1,1) the vacuum state is neutral Ba. The electron is then removed from the 6s orbital and allowed back into the 6s and 6p orbitals. Results when using X2C and 4c Hamiltonian, in combination with different basis sets (dyall.v3z and dyall.v4z) are compared to experiment. The excitation energies are shown in table 1 and 2 for sector (1,1) and sector (0,2), respectively.

Table 1: Energy levels of Ba in cm^{-1} compared to experiment, calculated with (1,1) sector FSCC method using X2C and 4c Hamiltonian and different basis sets.

Hamilt.	**Energy level**	**Exp. [26]**	**dyall.v3z**	**Diff. (%)**	**dyall.v4z**	**Diff. (%)**
X2C	$^3D_1$	*9033.9660*	11524.94185	28	9549.873742	6
	$^3D_2$	*9215.5010*	11720.35851	27	9764.632382	6
	$^3D_3$	*9596.533*	12146.79431	27	10214.23724	6
	$^1D_2$	*11395.350*	14095.03956	24	12456.61795	9
4c	$^3D_1$	*9033.9660*	11563.6457	28	9585.1200	6
	$^3D_2$	*9215.5010*	11757.9227	28	9798.9592	6
	$^3D_3$	*9596.533*	12181.36207	27	10245.94776	7
	$^1D_2$	*11395.350*	14131.62869	24	12492.35758	10

Table 2: Energy levels of neutral and ionized Ba in cm^{-1} compared to experiment, calculated with (0,2) sector FSCC method using 4c Hamiltonian and different basis sets.

Charge	Energy level	Exp. [26]	dyall.v3z	Diff. (%)	dyall.v4z	Diff. (%)
0	$^3D_1$	*9033.9660*	11045.9210	22	9813.2772	9
	$^3D_2$	*9215.5010*	11242.9500	22	10002.2740	9
	$^3D_3$	*9596.533*	11652.8716	21	10390.2902	8
	$^1D_2$	*11395.350*	13750.27335	21	12420.66336	9
+1	$^2D_{3/2}$	*4873.8520*	6534.2644	34	5864.8151	20
	$^2D_{5/2}$	*5674.8070*	7350.6583	30	6685.5171	18

In both table 1 and 2 it is clear that using a larger basis set gives a significant smaller difference with experiment. From table 1 one can see that there is not a large difference between using the four component upon the two component Hamiltonian.

Sector (1,1) and sector (0,2) give similar results for neutral Ba, though sector (1,1) is slightly more accurate. This can be explained by the fact that in sector (1,1) the starting point is the actual state of interest, while in sector (0,2) the starting point is the doubly ionized state. For the doubly ionized state, the DHF wavefunction will be a worse description of the system.

From the differences in table 2, one could argue that the calculated energy levels for the ionized atom are less accurate than for the neutral atom. This is actually not the case. The energies of the ionized states are smaller, giving a larger difference in percent, but the absolute differences are of the same order.

4.2 Cs

For Cs the polarizability of the ground state $^2S_{1/2}$ was calculated using different methods, X2C and 4c Hamiltonian and different basis sets. The results are compared to the experimental value of 401.2(7) a.u. [27] where the polarizability of Cs was measured using atom interferometry. In the FSCC method, the calculation was done in sector (0,1), where the vacuum state corresponds to ionized Cs. The results are shown in table 3.

Table 3: Calculated polarizability of Cs in a.u., using different methods and compared to experiment.

Hamilt.	Method	dyall.v2z	Diff. (%)	dyall.v3z	Diff. (%)	dyall.v4z	Diff. (%)
X2C	DHF	660.79	65	659.91	64	667.98	66
	CCSD	435.92	9	435.38	9	438.34	9
	CCSD(T)	416.31	4	406.67	1	405.05	1
	FSCC	415.02	3	409.95	2	408.46	2
	FSCC(nr)	484.61	21	483.88	21	485.79	21
4c	DHF	659.91	64	665.27	66	667.07	66
	CCSD	435.38	9	436.08	9	437.77	9
	CCSD(T)	415.82	4	406.23	1	404.54	1
	FSCC	414.53	3	409.45	2	409.96	2

The DHF results are not accurate, which is expected as electron correlation is not treated. The results get significantly better for CCSD(T) and FSCC, which give similar results. When looking at the CCSD and CCSD(T) results, the effect of including perturbative triple excitations becomes apparent. For the largest basis set, the difference between the two is around 8 percent, making it clear that triple excitations can be important to include. As in the Fock-Space Coupled Cluster method only single and double excitations are included, the results comply surprisingly well with CCSD(T).

The difference between X2C and 4c Hamiltonian calculations is minor, less than 1 percent. As the difference in results for dyall.v3z and dyall.v4z is small (smaller than 0.5 percent), it wouldn't be necessary to increase the basis set even further. The results are converged with respect to the basis set.

It is also interesting to look at the effects of relativity. Therefore, also a non-relativistic FSCC calculation is done (FSCC(nr) in the table). The non-relativistic results differ a lot from the relativistic ones. The relativistic polarizability is a lot smaller. This is probably caused by the relativistic contraction of the s-orbitals, making it more difficult to pull away the outer electron (which is in a s-orbital). This results in a smaller polarizability. From these results it becomes clear that taking into account relativity is really important when doing calculations on heavy systems.

4.3 MgH

This is an interesting system to look at, as it has the same ground state as CaF, SrF and BaF and similar behaviour can be expected. The parallel and perpendicular component of the polarizability of the ground state of MgH ($X^2\Sigma$) was calculated using different methods, 4c Hamiltonian and dyall.v4z basis set. An experimental equilibrium internuclear bond length of 1.73 Å [26] was used. The results are shown in table 4 and compared to other theoretical work [28].

Table 4: Perpendicular (α_{xx}) and parallel (α_{zz}) polarizabilities of MgH, using 4c Hamiltonian and dyall.v4z basis set, compared to other theoretical work.

Method	α_{zz} (this work)	α_{zz} [28]	α_{xx} (this work)	α_{xx} [28]
DHF	52.91	56.50	64.78	69.63
CCSD	54.89	58.22	62.51	68.77
CCSD(T)	54.88	58.47	62.44	68.75
FSCC	55.59	-	62.43	-

The results of this work for CCSD(T) and FSCC are similar. The results of this work for DHF, CCSD and CCSD(T) agree well with the results of the other work. The difference can be explained by the fact that in the other work a non-relativistic program (GAUSSIAN-92) and a smaller basis set is used. This basis set consists out of 85 contracted gaussian-type functions. For Mg a basis set is used [29] where diffuse and polarization functions are added, in total: 14s9p3d2f/7s5p3d2f. For H a basis set is used [30] where diffuse and polarization functions are added, in total: 11s6p2d/6s6p2d4.

As a comparison, in the dyall.v4z basis set Mg is described by large components 25s15p7d5f3g and small components 15s32p20d10f5g3h and H by large components 11s3p2d1f and small components 3s13p4d2f1g.

4.4 Rb

For Rb the energy levels of the first two excited states ($^2P_{1/2}$, $^2P_{3/2}$) as well as the polarizability of the ground ($^2S_{1/2}$) and first two excited states were calculated with the FSCC method. The 4c Hamiltonian is used, in combination with different basis sets, with and without diffuse functions.

Due to the applied electric field in the polarizability calculation, the $^2P_{3/2}$ state is split up into two. From these two levels the average was taken. For the largest basis sets (tabel 6), the difference in polarizability of the two levels is around 333 atomic units.

The results are shown in table 5, 6 and 7 compared to other theoretical work [31] and experiment [26], [32], [27]. The differences in percent are between this work and the experiment. In the theoretical work they used relativistic many-body perturbation theory.

Table 5: Calculated polarizability of ground state and first excited states of Rb in a.u., using FSCC method in combination with 4c Hamiltonian and different basis sets. The results are compared to other theoretical work and experiment. The differences in percent are between this work and experiment.

State	**dyall.v2z**	**Diff. (%)**	**dyall.v3z**	**Diff. (%)**	**dyall.v4z**	**Diff. (%)**	**Other work [31]**	**Exp.**
$^2S_{1/2}$	322.74	0.8	322.31	0.7	321.40	0.4	-	*320.1(6)*[27]
$^2P_{1/2}$	64.47	92.1	355.16	56.2	699.47	13.8	807	*811(6)*[32]
$^2P_{3/2}$	79.09	90.8	379.37	55.8	747.55	12.7	870	*858(7)*[32]

In table 5, one thing that can be noticed is that for the largest basis set, the differences between the excited states and experiment is still quite large, around 13 percent. To reduce this difference, diffuse functions are added to the dyall.v4z basis set, creating an even larger basis set. The results are shown in table 6. The difference already reduces to about 1 percent when only one diffuse function is added. The reason why diffuse functions are in particular important for excited states stems from the fact that the excited states extend further from the nucleus, with respect to the ground state. A better description for electrons far away from the nucleus is therefore extra important.

Table 6: Calculated polarizability of ground state and first excited states of Rb in a.u., using FSCC method in combination with 4c Hamiltonian and dyall.v4z basis sets with diffuse functions added. The results are compared to other theoretical work and experiment. The differences in percent are between this work and experiment.

State	**s-aug dyall.v4z**	**Diff. (%)**	**d-aug dyall.v4z**	**Diff. (%)**	**t-aug dyall.v4z**	**Diff. (%)**	**Other work [31]**	**Exp.**
$^2S_{1/2}$	321.55	0.5	321.55	0.5	321.55	0.5	-	*320.1(6)*[27]
$^2P_{1/2}$	800.45	1.3	802.93	1.0	803.24	1.0	807	*811(6)*[32]
$^2P_{3/2}$	861.52	0.4	864.25	0.7	864.605	0.8	870	*858(7)*[32]

Table 7: Calculated excitation energies of the first two excited states of Rb in cm^{-1}, using FSCC method in combination with 4c Hamiltonian and dyall.v4z basis set with diffuse functions added. The results are compared to experiment.

State	**s-aug dyall.v4z**	**Diff. (%)**	**d-aug dyall.v4z**	**Diff. (%)**	**t-aug dyall.v4z**	**Diff. (%)**	**Exp. [26]**
$^2P_{1/2}$	12546.76	0.3	12546.63	0.3	12546.64	0.3	*12578.95*
$^2P_{3/2}$	12785.16	0.2	12785.02	0.3	12785.03	0.3	*12816.55*

The results for the excitation energies when using a large basis set with diffuse functions agree very well with experiment. As the difference between s-aug-dyall.v4z and d-aug-dyall.v4z is small, it can be concluded that the calculation is converged at the s-aug-dyall.v4z basis set (single diffuse function).

One thing that stands out from table 6 is that the polarizability of the excited states is a lot larger than that of the ground state. This can be explained by the fact that in the ground state, the outer electron is in a s-orbital and in the excited states it is in a p-orbital. The p-orbital extends out further from the nucleus, making it easier to pull it away by an external electric field. This results in a larger polarizability for the excited states.

4.5 LiH

The perpendicular and parallel polarizability component of LiH were calculated of the ground ($X^1\Sigma$) and excited state ($A^1\Sigma$), using the FSCC method. The 4c Hamiltonian in combination with dyall.v4z basis set was used. For the ground state and the excited state an experimental equilibrium bond length of 1.5949 Å [33] and 2.559 Å [34] was used, respectively. The results are shown in table 8 and compared to other theoretical work [34], where they used CCSD(T) method for the ground state and time-dependent gauge invariant method (TDGI) for the excited state. They used Jeung's original basis set [35] including diffuse functions consisting of contracted [7s,5p,3d,1f] and [7s,5p,5d,2f], for Li and H, respectively.

Also, the excitation energy of the first excited state of LiH was calculated using dyall.v4z, 4c Hamiltonian and FSCC method. The result is 26497.48 cm^{-1}. Compared to the experimental value of 26516 cm^{-1} [36] this gives a difference of 0.07 percent.

Table 8: Calculated parallel and perpendicular polarizability component of ground state and first excited state of LiH in a.u., using FSCC method in combination with 4c Hamiltonian and dyall.v4z basis set. The results are compared to other theoretical work.

State	α_{zz} (this work)	α_{zz} [34]	α_{xx} (this work)	α_{xx} [34]
$X^1\Sigma$	25.186	27.04	28.654	29.96
$A^1\Sigma$	56.826	57.69	169.99	177.27

The results of this work agree well with the other work, where the differences are due to the different methods and basis sets used.

One thing that stands out is the large difference between the parallel and perpendicular component of the excited state, where for the ground state the two components are very similar. An explanation

for this could be the shape of the valence molecular orbitals. The ground state is made mostly from the s-orbital of H. In the excited state, the $d_{x^2-y^2}$-orbital of Li contributes to the valence molecular orbital. This $d_{x^2-y^2}$-orbital extends in the x-direction, more than in the z-direction. This makes it easier to pull the electron away from the nucleus with an external electric field in the x-direction. Because of that, the polarizability component in the x-direction (the perpendicular component α_{xx}) is larger than the parallel component.

5 Results

In this section, the results of the parallel and perpendicular component of the polarizability of CaF, SrF and BaF are presented. Calculations were done for the ground state $X^2\Sigma$ and first five excited states $^2\Delta_{3/2}$, $^2\Delta_{5/2}$, $^2\Pi_{1/2}$, $^2\Pi_{3/2}$ and $B^2\Sigma$. All calculations were done using the FSCC method with the two component X2C Hamiltonian. Four component Hamiltonian calculations are not done, because the difference between two and four component results are very small, while computational effort increases a lot when using the four component Hamiltonian. This was already shown for Ba and Cs and it will be shown for BaF in this section.

The molecules have an unpaired electron in the valence shell. Therefore, sector (0,1) calculations were done, where the vacuum state corresponds to BaF^+, SrF^+ and CaF^+. In the calculations, electric fields ranging from -0.00005 to 0.00005 a.u. were used.

Each state has a different internuclear distance. To reduce computational effort, calculations were first done in ground state geometry, i.e. using the equilibrium internuclear distance of the ground state. This can be done because for the molecules of interest, the ground state geometry is very similar to the excited state geometries. In the ground state geometry, convergence with respect to the basis set and diffuse function was tested. Also, calculations with all electrons correlated are compared to calculations with frozen core. In the latter, some of the core electrons are not included in the calculations, decreasing computational effort. In the end, the calculations were performed on each state using the appropriate internuclear distance.

The internuclear distances used for the different states of the molecules are given in table 9. The ones in cursive are from experiment [26], the other ones are obtained in FSCC calculations done by Yongliang Hao [37].

Table 9: Internuclear distances in Å used for the different states of the molecules.

State	**CaF**	**SrF**	**BaF**
$X^2\Sigma$	*1.967*	*2.0753*	*2.162*
$^2\Delta_{3/2}$	1.995	2.099	2.207
$^2\Delta_{5/2}$	1.995	2.098	2.205
$^2\Pi_{1/2}$	1.994	*1.952*	*2.183*
$^2\Pi_{3/2}$	1.994	*1.952*	*2.183*
$B^2\Sigma$	1.961	*2.0801*	*2.208*

It has already been shown for Rb that adding diffuse functions to the basis set has a large effect on the polarizability results, especially for excited states. The same turned out to be true for CaF, SrF and BaF. Therefore, in most cases only the results for basis sets with diffuse functions are presented. As was also done in some of the preparation work, calculations are done for different number of diffuse functions added to the largest basis set. If the difference in results between two cases is small, one can say that the results are converged with respect to diffuse functions. At that point, it is not needed to add even more diffuse functions to obtain better results.

5.1 CaF

Before showing the results of the parallel and perpendicular component of the polarizability, the calculated excitation energies T_e are presented. For these energies, experimental values [38] are available. This gives the opportunity to check the calculations that are done, whereas for the polarizability there is no experiment available. The energies are calculated using the FSCC method with the X2C Hamiltonian and t-aug-dyall.v4z basis set.

Table 10: Calculated excitation energies first five excited states of CaF in cm^{-1}, using FSCC method in combination with X2C Hamiltonian and t-aug-dyall.v4z basis set. All electrons were included in the calculation.

State	$\mathbf{T_e}$	**Exp. [38]**	**Diff. (%)**
$A^2\Pi_{1/2}$	16733.923	*16529.134*	1.2
$A^2\Pi_{3/2}$	16810.855	*16529.134*	1.7
$B^2\Sigma$	19368.761	*18833.152*	2.8
$B'^2\Delta_{3/2}$	22764.859	*21573.930*	5.5
$B'^2\Delta_{5/2}$	22786.582	*21573.930*	5.6

The difference for the Δ states is the largest. A reason for this can be that the calculation for these states aren't fully converged yet for the t-aug-dyall.v4z basis set, as will be shown later in this section.

5.1.1 Parallel component

First, the dependence of the polarizability on the basis set is tested. The calculations were done using s-aug-dyall.v2z, s-aug-dyall.v3z and s-aug-dyall.v4z basis sets. For each state, the trend is shown in figure 5. As the $A^2\Pi_{1/2}$ and $A^2\Pi_{3/2}$ states as well as the $B'^2\Delta_{3/2}$ and $B'^2\Delta_{5/2}$ states are very similar (because the spin-orbit coupling is small), they are right on top of each other in the figure.

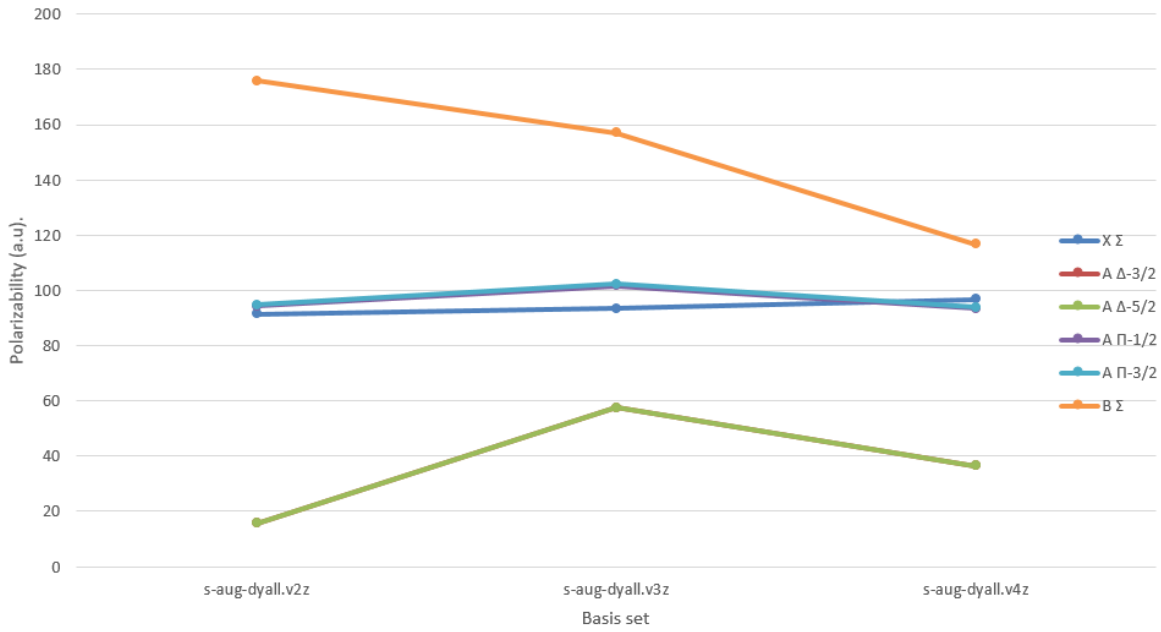

Figure 5: Parallel polarizability in a.u. of the different states of CaF using different basis sets with diffuse functions.

This figure shows a somewhat unexpected trend. If one increases the basis set, the results of the calculations will be more accurate. At some point, increasing the basis set will not give different results: the results are converged. Therefore, the trends shown in figure 5 are unexpected, as the polarizability of some states does not converge to a certain number. To figure out if something is going wrong, calculations were done for the basis sets without diffuse function added. The results are shown in figure 6.

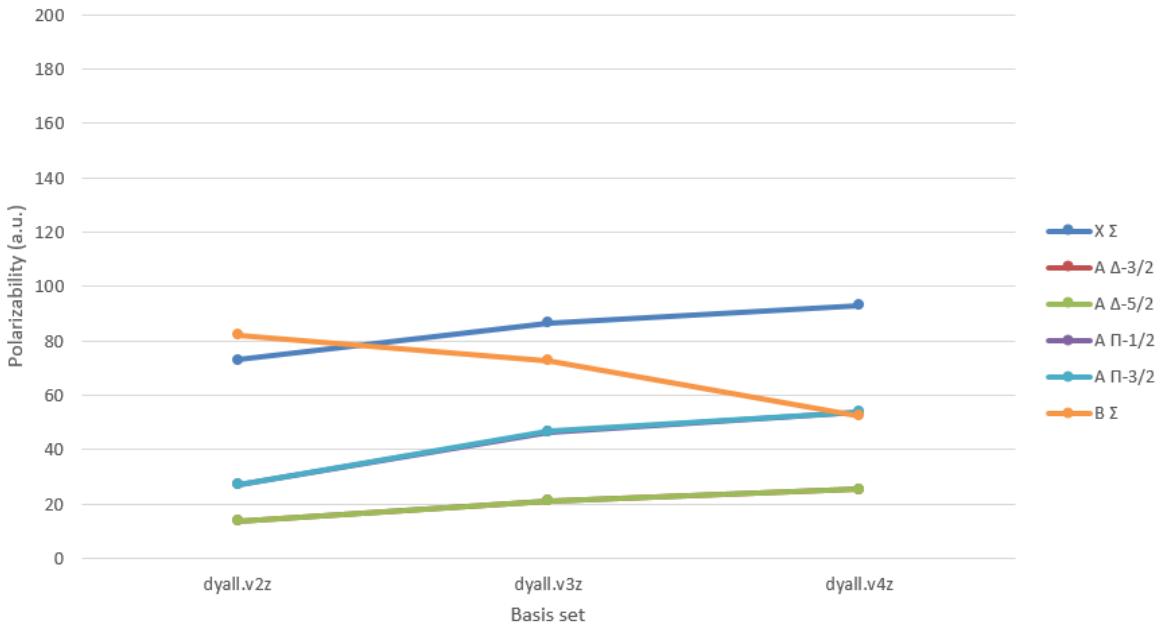

Figure 6: Parallel polarizability in a.u. of the different states of CaF using different basis sets without diffuse functions.

The trends in figure 6 look like expected: the results converge with respect to increasing basis set. From this can be concluded that something is going wrong when the diffuse functions are added. The absolute differences in a.u. between the basis sets with and without a single diffuse function are shown in table 11. These are the differences between the values from figure 5 and 6.

Table 11: Absolute differences in a.u. between the basis sets with and without a single diffuse function, so the differences between the values from figure 5 and 6.

State	**dyall.v2z**	**dyall.v3z**	**dyall.v4z**
$X^2\Sigma$	19	7	3
$A^2\Pi_{1/2}$	67	55	39
$A^2\Pi_{3/2}$	68	56	40
$B^2\Sigma$	94	84	64
$B'^2\Delta_{3/2}$	2	37	11
$B'^2\Delta_{5/2}$	2	37	11

It becomes clear that (in the case of the first 4 states), the larger the basis set, the less influence adding a diffuse function has. This is as expected, as a larger basis set already describes the electrons further away from the nucleus better than a smaller basis set. For the Δ states, one can see that something is off for the dyall.v2z basis set, as very little happens when adding a diffuse function. Because of this, the trend for the diffuse functions is not as expected.

In table 12 the results for the parallel component of the polarizability are shown for the dyall.v4z basis set with a single, double and triple diffuse function added. The stated differences in percent are

between the results of the d-aug-dyall.v4z and t-aug-dyall.v4z basis set.

Table 12: Calculated parallel polarizability components of ground state and first five excited states of CaF in a.u., using FSCC method in combination with X2C Hamiltonian and s-aug-dyall.v4z, d-aug-dyall.v4z and t-aug-dyall.v4z basis set. In all calculations, all electrons were correlated. The calculations were done in ground state geometry. The stated difference is between d- and t-aug-dyall.v4z.

State	s-aug-dyall.v4z	d-aug-dyall.v4z	t-aug-dyall.v4z	Diff. (%)
$X^2\Sigma$	95.91	97.72	96.50	1.3
$A^2\Pi_{1/2}$	92.65	101.61	101.01	0.6
$A^2\Pi_{3/2}$	93.18	102.30	101.68	0.6
$B^2\Sigma$	116.53	137.28	137.12	0.1
$B'^2\Delta_{3/2}$	35.66	47.16	50.67	7.0
$B'^2\Delta_{5/2}$	35.72	47.16	50.86	7.0

As the differences between d-aug-dyall.v4z and t-aug-dyall.v4z are small, not much deviation in results is expected when adding even more diffuse functions. In table 13 the results for all electron correlated are compared to results for frozen core calculations.

Table 13: Calculated parallel polarizability components of ground state and first five excited states of CaF in a.u., using FSCC method in combination with X2C Hamiltonian and d-aug-dyall.v4z basis set. All electron calculations are compared to calculations with 16 electrons correlated. The calculations were done in ground state geometry.

State	28 electrons (all)	16 electrons	Diff. (%)
$X^2\Sigma$	95.95	96.72	0.4
$A^2\Pi_{1/2}$	99.61	100.17	0.6
$A^2\Pi_{3/2}$	100.31	100.86	0.6
$B^2\Sigma$	134.60	135.83	0.9
$B'^2\Delta_{3/2}$	45.07	45.72	1.4
$B'^2\Delta_{5/2}$	45.19	45.84	1.4

The difference between all electron and frozen core calculations is small, but there is also not a large computational time difference. It was therefore decided to do the final calculations with t-aug-dyall.v4z basis set and all electrons correlated. The results are shown in table 14.

Table 14: Calculated parallel polarizability components of ground state and first five excited states of CaF in a.u. in their own geometry, using FSCC method in combination with X2C Hamiltonian and t-aug-dyall.v4z basis set. All electrons were included in the calculation.

State	Parallel polarizability (a.u.)
$X^2\Sigma$	96.61
$A^2\Pi_{1/2}$	101.80
$A^2\Pi_{3/2}$	102.50
$B^2\Sigma$	138.43
$B'^2\Delta_{3/2}$	47.96
$B'^2\Delta_{5/2}$	48.14

One thing that could be interesting to look at, is the effect of the geometry used on the results. In

table 15, the results for the ground state geometry and the results for the states in their equilibrium geometry are compared. Small differences are observed.

Table 15: Differences in percent between the results when using ground state geometry (α_{ground}) and when using the proper equilibrium geometries for the states ($\alpha_{\text{equil.}}$) for CaF. Also, the used equilibrium distances are shown.

State	α_{ground}	$\alpha_{\text{equil.}}$	**Diff. (%)**	**Equil. distance used (Å)**
$X^2\Sigma$	96.61	96.61	0	1.967
$A^2\Pi_{1/2}$	100.85	101.80	0.9	1.994
$A^2\Pi_{3/2}$	101.52	102.50	1.0	1.994
$B^2\Sigma$	136.28	138.43	1.6	1.961
$B'^2\Delta_{3/2}$	50.34	47.96	5.0	1.995
$B'^2\Delta_{5/2}$	50.52	48.14	4.9	1.995

5.1.2 Perpendicular component

In the perpendicular calculations the electric field is directed perpendicular to the internuclear axis. Because of this, there are more symmetry restrictions than for the parallel calculations. This makes the calculations computationally a lot more challenging. For that reason, it hasn't been possible to check and/or reach convergence with respect to basis set and diffuse functions.

In table 16 the results for the perpendicular components of the polarizability are shown for s-aug-dyall.v3z and s-aug-dyall.v4z basis sets. For the smaller basis set s-aug-dyall.v2z the calculations didn't work properly, as the FSCC iterations didn't converge.

Table 16: Calculated perpendicular polarizability components of ground state and first five excited states of CaF in a.u., using FSCC method in combination with X2C Hamiltonian and s-aug-dyall.v3z and s-aug-dyall.v4z basis set. In both calculations, 16 electrons were correlated. The calculations were done in ground state geometry.

State	**s-aug-dyall.v3z**	**s-aug-dyall.v4z**	**Diff. (%)**
$X^2\Sigma$	147.08	149.26	1.5
$A^2\Pi_{1/2}$	204.11	200.82	1.6
$A^2\Pi_{3/2}$	206.53	203.56	1.5
$B^2\Sigma$	142.89	131.46	8.7
$B'^2\Delta_{3/2}$	-17.41	-70.72	75.4
$B'^2\Delta_{5/2}$	-18.49	-72.19	73.8

There is a large difference between s-aug-dyall.v3z and s-aug-dyall.v4z basis set, which implies that the calculations aren't converged with respect to basis set yet or more diffuse functions need to be added. Unfortunately, due to computational limits this wasn't possible to do.

In table 17 the differences between all electrons and frozen core calculations are shown. A small difference arises from using a frozen core.

Table 17: Calculated perpendicular polarizability components of ground state and first five excited states of CaF in a.u., using FSCC method in combination with X2C Hamiltonian and s-aug-dyall.v4z basis set. All electron calculations are compared to calculations with 16 electrons correlated. The calculations were done in ground state geometry.

State	28 electrons (all)	16 electrons	Diff. (%)
$X^2\Sigma$	149.46	149.26	0.1
$A^2\Pi_{1/2}$	202.36	200.82	0.8
$A^2\Pi_{3/2}$	205.15	203.56	0.8
$B^2\Sigma$	131.74	131.46	0.2
$B'^2\Delta_{3/2}$	-72.00	-70.72	1.8
$B'^2\Delta_{5/2}$	-73.47	-72.19	1.7

One thing that stands out is the fact that the polarizability for the Δ states is negative. This turns out to be the case for the other molecules as well. This can be understood by using the sum-over-states polarizability description [39]:

$$\alpha_a = \frac{2}{3} \sum_{n \neq a} \frac{|\mu_{\mathrm{na}}|^2}{\Delta E_{\mathrm{na}}} \tag{57}$$

Here, a is the state for which the polarizability is calculated, μ_{na} is the transition dipole moment between the states a and n and ΔE_{na} is the difference in energy between states a and n. Viewed in this way, it can be seen that the other states contribute to the polarizability of state a. How large these contributions are depends on the amount of mixing with state a and the other states. In contrary to the ground state, an excited state can mix with a lower lying state. This results in a negative contribution to the polarizability, sometimes leading to an overall negative polarizability component [39]. In the case of the $^2\Delta$ states, the negative polarizability could be the consequence of strong mixing with the lower lying states.

5.2 SrF

In table 18 the excitation energies for SrF are shown, compared to experiment [40] where available. The calculations are done using the d-aug-dyall.v4z basis set and 34 electrons correlated. There is good agreement.

Table 18: Calculated excitation energies first five excited states of SrF in cm^{-1}, using FSCC method in combination with X2C Hamiltonian and d-aug-dyall.v4z basis set. 34 electrons were included in the calculation.

State	$\mathbf{T_e}$	Exp. [40]	Diff. (%)
$A^2\Pi_{1/2}$	15105.6	*15068.9*	0.2
$A^2\Pi_{3/2}$	15389.5	*15348.9*	0.3
$B^2\Sigma$	17423.6	*172301.9*	0.9
$B'^2\Delta_{3/2}$	19267.20	-	-
$B'^2\Delta_{5/2}$	19392.17	-	-

5.2.1 Parallel component

Also for SrF, the dependence of the parallel component of the polarizability on the basis set is tested and the results are in figure 7. In contrast with CaF, the trends when using diffuse functions actually look as expected. There is convergence with respect to the basis set.

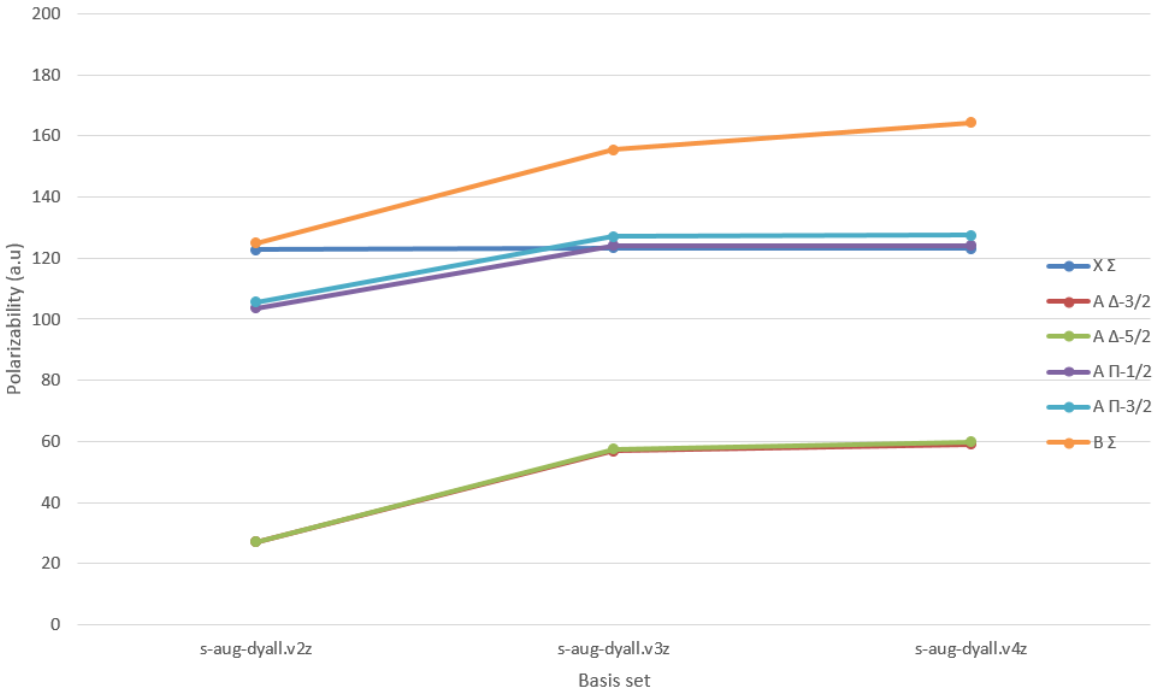

Figure 7: Parallel polarizability SrF using different basis sets with diffuse functions.

In table 17, results are shown for dyall.v4z basis set adding diffuse functions. Considering the small difference between d-aug-dyall.v4z and t-aug-dyall.v4z basis set, one can conclude that the results are converged at the d-aug-dyall.v4z basis set.

Table 19: Calculated parallel polarizability components of ground state and first five excited states of SrF in a.u., using FSCC method in combination with X2C Hamiltonian and s-aug-dyall.v4z, d-aug-dyall.v4z and t-aug-dyall.v4z basis set. In all calculations, 16 electrons were correlated. The calculations were done in ground state geometry. The stated difference is between d- and t-aug-dyall.v4z.

State	s-aug-dyall.v4z	d-aug-dyall.v4z	t-aug-dyall.v4z	Diff. (%)
$X^2\Sigma$	123.36	123.57	123.60	0.1
$A^2\Pi_{1/2}$	123.77	128.51	129.40	0.7
$A^2\Pi_{3/2}$	127.18	132.26	133.40	0.8
$B^2\Sigma$	163.18	170.76	171.30	0.3
$B'^2\Delta_{3/2}$	58.73	63.53	63.50	0.1
$B'^2\Delta_{5/2}$	59.46	64.57	64.60	0.0

In table 20 the difference between the results of all electron and frozen core calculations is shown.

Table 20: Calculated parallel polarizability components of ground state and first five excited states of SrF in a.u., using FSCC method in combination with X2C Hamiltonian and s-aug-dyall.v4z basis set. All electron calculations are compared to calculations with 34 electrons correlated. The calculations were done in ground state geometry.

State	46 electrons (all)	34 electrons	Diff. (%)
$X^2\Sigma$	123.05	123.10	0.0
$A^2\Pi_{1/2}$	124.12	124.18	0.1
$A^2\Pi_{3/2}$	127.56	127.62	0.1
$B^2\Sigma$	164.27	164.39	0.1
$B'^2\Delta_{3/2}$	59.18	59.18	0.0
$B'^2\Delta_{5/2}$	59.84	59.91	0.1

Since the difference is very small, the final calculations are done using this frozen core, in combination with d-aug-dyall.v4z basis set. The results are shown in table 15.

Table 21: Calculated parallel polarizability components of ground state and first five excited states of SrF in a.u. in their own geometry, using FSCC method in combination with X2C Hamiltonian and d-aug-dyall.v4z basis set. There are 34 electrons included in the calculations.

State	Parallel polarizability (a.u.)
$X^2\Sigma$	123.29
$A^2\Pi_{1/2}$	129.79
$A^2\Pi_{3/2}$	133.62
$B^2\Sigma$	170.07
$B'^2\Delta_{3/2}$	62.80
$B'^2\Delta_{5/2}$	63.86

For the ground state polarizability, there is other theoretical work known. 125 a.u. [41] and 126 a.u. [42] have been obtained using the CCSD(T) method, in good agreement with the result presented here.

In table 21, the results for the ground state geometry and the results for the states in their equilibrium geometry are compared. Small differences are observed. The largest difference is obtained for the $^2\Pi$ states, which can be explained by the large difference between the ground state equilibrium distance and the actual equilibrium distance.

Table 22: Differences in percent between the results when using ground state geometry (α_{ground}) and when using the proper equilibrium geometries for the states ($\alpha_{\text{equil.}}$) for SrF. Also, the used equilibrium distances are shown.

State	α_{ground}	$\alpha_{\text{equil.}}$	Diff. (%)	Equil. distance used (Å)
$X^2\Sigma$	123.29	123.29	0.0	2.0753
$A^2\Pi_{1/2}$	128.92	129.79	2.2	1.952
$A^2\Pi_{3/2}$	132.70	133.62	2.1	1.952
$B^2\Sigma$	172.00	170.07	0.7	2.0801
$B'^2\Delta_{3/2}$	64.17	62.80	0.7	2.099
$B'^2\Delta_{5/2}$	65.23	63.86	1.1	2.098

5.2.2 Perpendicular component

In figure 8 the dependence of the perpendicular components of the polarizability on the size of the basis set with diffuse functions is shown. Again, there is convergence with respect to basis set.

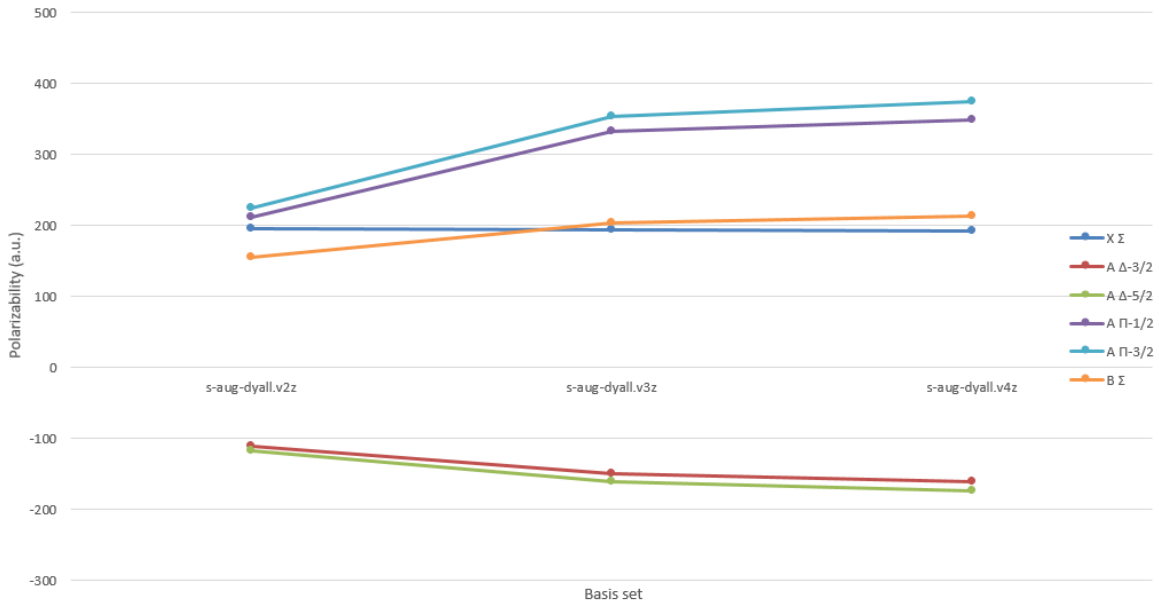

Figure 8: Perpendicular polarizability SrF using different basis sets with diffuse functions.

In table 23 the results are shown for s-aug-dyall.v4z and d-aug-dyall.v4z basis sets. In table 24 the results for all electron and frozen core calculations are shown.

Table 23: Calculated perpendicular polarizability components of ground state and first five excited states of SrF in a.u., using FSCC method in combination with X2C Hamiltonian and s-aug-dyall.v4z and d-aug-dyall.v4z basis set. In both calculations, 16 electrons were correlated. The calculations were done in ground state geometry.

State	**s-aug-dyall.v4z**	**d-aug-dyall.v4z**	**Diff. (%)**
$X^2\Sigma$	192.87	193.09	0.1
$A^2\Pi_{1/2}$	349.11	349.00	0.0
$A^2\Pi_{3/2}$	373.86	373.00	0.2
$B^2\Sigma$	213.13	221.27	3.7
$B'^2\Delta_{3/2}$	-161.48	-152.75	5.7
$B'^2\Delta_{5/2}$	-173.53	-164.30	5.6

Table 24: Calculated perpendicular polarizability components of ground state and first five excited states of SrF in a.u., using FSCC method in combination with X2C Hamiltonian and s-aug-dyall.v3z basis set. All electron calculations are compared to calculations with 16 electrons correlated. The calculations were done in ground state geometry.

State	46 electrons (all)	16 electrons	Diff. (%)
$X^2\Sigma$	192.94	193.12	0.1
$A^2\Pi_{1/2}$	329.81	331.68	0.6
$A^2\Pi_{3/2}$	351.86	353.95	0.6
$B^2\Sigma$	204.55	204.14	0.2
$B'^2\Delta_{3/2}$	-145.98	-149.27	2.3
$B'^2\Delta_{5/2}$	-157.05	-160.49	2.2

The difference between the two basis sets is still on the large side for the last three states in table 23. Also, the differences for the Δ states in table 24 are on the large side. Due to the large computational time and costs, it is not feasible to add more diffuse functions or include all electrons in the final calculations. For that reason, the final calculations were done with s-aug-dyall.v4z basis set in combination with the frozen core. The results for the states in their own geometry are shown in table 25.

Table 25: Calculated perpendicular polarizability components of ground state and first five excited states of SrF in a.u. in their own geometry, using FSCC method in combination with X2C Hamiltonian and s-aug-dyall.v4z basis set. There were 16 electrons included in the calculations.

State	Perpendicular polarizability (a.u.)
$X^2\Sigma$	192.87
$A^2\Pi_{1/2}$	350.24
$A^2\Pi_{3/2}$	375.05
$B^2\Sigma$	209.94
$B'^2\Delta_{3/2}$	-161.05
$B'^2\Delta_{5/2}$	-173.10

Also for the perpendicular component of the ground state there is other theoretical work availabe. In reference [41] they obtained an average polarizability $\bar{\alpha}$ of 170.05 a.u. For the parallel component they obtained 125 a.u. The perpendicular component can be calculated using the equation:

$$\bar{\alpha} = \frac{1}{3}(\alpha_{zz} + 2\alpha_{xx}) \tag{58}$$

So, they got a value of 192.58 a.u. for the perpendicular component, again in good agreement with the result presented here.

5.3 BaF

In table 26 the results for the calculated excitation energies for BaF are shown, compared to experiment. The calculations were done using the d-aug-dyall.v4z basis set and 34 electrons correlated. Again, for the Δ states the difference with experiment is the largest.

Table 26: Calculated excitation energies first five excited states of BaF in cm^{-1}, using FSCC method in combination with X2C Hamiltonian and d-aug-dyall.v4z basis set. 34 electrons were included in the calculations.

State	T_e	Exp.	Diff. (%)
$A'^2\Delta_{3/2}$	11162.465	*10733.59* [43]	4.0
$A'^2\Delta_{5/2}$	11588.488	*11144.59* [43]	4.0
$A^2\Pi_{1/2}$	11743.176	*11646.90* [44]	0.8
$A^2\Pi_{3/2}$	12386.69	*12278.20* [44]	0.9
$B^2\Sigma$	14220.14	*14062.52* [43]	1.1

5.3.1 Parallel component

For the parallel component of the polarizability of BaF with respect to increasing basis set with a diffuse function added, similar trends as for CaF were observed. Because the calculations using basis sets without diffuse functions gave unexpected results for BaF, a similar comparison as was done for CaF couldn't be done and the reason for the unexpected trend might not be the same.

It has already been shown for Cs and Ba that using the four component or two component Hamiltonian does not matter that much for polarizability calculations. To be sure, this has also been tested for BaF as well. In tabel 27 the results for calculations using s-aug-dyall.v4z basis set in combination with four and two component Hamiltonian are presented.

Table 27: Calculated parallel polarizability components of ground state and first five excited states of BaF in a.u., using FSCC method in combination with X2C and 4c Hamiltonian and s-aug-dyall.v4z basis set. In both calculations, 16 electrons were correlated. The calculations were done in ground state geometry.

State	X2C	4c	Diff. (%)
$X^2\Sigma$	171.95	171.78	0.1
$A^2\Delta_{3/2}$	64.70	64.96	0.4
$A^2\Delta_{5/2}$	59.83	59.88	0.1
$A'^2\Pi_{1/2}$	132.97	133.08	0.1
$A'^2\Pi_{3/2}$	135.56	135.53	0.0
$B^2\Sigma$	173.47	173.85	0.2

The difference between the two Hamiltonians is smaller than 0.5 percent. Because the four component calculations took twice as long as the two component ones, it was chosen not to use the four component Hamiltonian.

In table 28 the results are shown for s-aug-dyall.v4z and d-aug-dyall.v4z. In table 29 the results of all electron and frozen core calculations are presented.

Table 28: Calculated parallel polarizability components of ground state and first five excited states of BaF in a.u., using FSCC method in combination with X2C Hamiltonian and s-aug-dyall.v4z and d-aug-dyall.v4z basis set. In both calculations, 16 electrons were correlated. The calculations were done in ground state geometry.

State	s-aug-dyall.v4z	d-aug-dyall.v4z	Diff. (%)
$X^2\Sigma$	171.95	171.92	0.0
$A^2\Delta_{3/2}$	64.697	65.3	0.9
$A^2\Delta_{5/2}$	59.826	60.637	1.3
$A'^2\Pi_{1/2}$	132.97	133.41	0.3
$A'^2\Pi_{3/2}$	135.56	136.6	0.8
$B^2\Sigma$	173.47	180.93	4.1

Table 29: Calculated parallel polarizability components of ground state and first five excited states of BaF in a.u., using FSCC method in combination with X2C Hamiltonian and s-aug-dyall.v4z basis set. All electron calculations are compared to calculations with 34 electrons correlated. The calculations were done in ground state geometry.

State	64 electrons (all)	34 electrons	Diff. (%)
$X^2\Sigma$	170.40	170.20	0.1
$A^2\Delta_{3/2}$	67.722	67.13	0.9
$A^2\Delta_{5/2}$	60.239	59.853	0.6
$A'^2\Pi_{1/2}$	134.02	132.88	0.9
$A'^2\Pi_{3/2}$	134.11	133.11	0.8
$B^2\Sigma$	175.08	172.95	1.2

As the difference for the $B^2\Sigma$ state in table 28 is on the large side and the difference between all electron and frozen core calculations is small, the final calculations were done with this frozen core in combination with d-aug-dyall.v4z basis set. The results are shown in table 30.

Table 30: Calculated parallel polarizability components of ground state and first five excited states of BaF in a.u. in their own geometry, using FSCC method in combination with X2C Hamiltonian and d-aug-dyall.v4z basis set. There were 34 electrons included in the calculations.

State	Parallel polarizability (a.u.)
$X^2\Sigma$	170.06
$A^2\Delta_{3/2}$	66.50
$A^2\Delta_{5/2}$	59.54
$A'^2\Pi_{1/2}$	128.81
$A'^2\Pi_{3/2}$	129.52
$B^2\Sigma$	153.92

In table 31 the results for the ground state geometry and the results for the states in their equilibrium geometry are compared. It can be seen that the geometry used has a very large impact on the result of the $B^2\Sigma$ state. Such a large difference was not observed for CaF or SrF. A reason for this could be that the relative change from going to the ground state equilibrium bond length to the $B^2\Sigma$ state equilibrium bond length is largest for BaF (about 2 percent against 0.3 percent, see table 9). One could argue that this is also the case for some other states, and there the difference between ground state

geometry and equilibrium geometry calculations is not that large. That could have something to do with the fact that the $B^2\Sigma$ state is formed mostly from the d_{z^2}-orbital of Ba (see section 'Discussion'), which extends along the z-axis. Elongating the bond length (which is also along the z-axis) can give a large difference, as the electron will feel less attraction from one of the nuclei, which is now further away. For other states made from orbitals that do not extend that much along the z-axis, it will have less impact.

Table 31: Differences in % between the results when using ground state geometry (α_{ground}) and when using the proper equilibrium geometries for the states ($\alpha_{\text{equil.}}$) for BaF. Also, the used equilibrium distances are shown.

State	α_{ground}	$\alpha_{\text{equil.}}$	**Diff. (%)**	**Equil. distance used (Å)**
$X^2\Sigma$	170.06	170.06	0.0	2.162
$B'^2\Delta_{3/2}$	67.64	66.50	1.7	2.207
$B'^2\Delta_{5/2}$	60.62	59.54	1.8	2.205
$A^2\Pi_{1/2}$	133.26	128.81	3.5	2.183
$A^2\Pi_{3/2}$	134.11	129.52	3.5	2.183
$B^2\Sigma$	180.17	153.92	17.1	2.208

5.3.2 Perpendicular component

As was stated before, due to the large computationally effort needed for the perpendicular component, it's challenging to do the calculations with large basis sets. For BaF, s-aug-dyall.v3z was the largest basis set reached. The results for s-aug-dyall.v2z and s-aug-dyall.v3z with all electrons correlated are shown in table 32.

Table 32: Calculated perpendicular polarizability components of ground state and first five excited states of BaF in a.u., using FSCC method in combination with X2C Hamiltonian and s-aug-dyall.v2z and s-aug-dyall.v3z basis set. All electrons were correlated. The calculations were done in ground state geometry.

State	**s-aug-dyall.v2z**	**d-aug-dyall.v3z**
$X^2\Sigma$	287.64	278.16
$A^2\Delta_{3/2}$	-197.13	-1761.00
$A^2\Delta_{5/2}$	-507.41	1892.00
$A'^2\Pi_{1/2}$	542.93	-4044.50
$A'^2\Pi_{3/2}$	663.82	4218.90
$B^2\Sigma$	51.99	210.17

Exept for the ground state and maybe the $B^2\Sigma$ state, the numbers in table 32 are quite strange. For s-aug-dyall.v2z there is a very large difference between the two Δ states, something that wasn't observed for CaF and SrF. Because the s-aug-dyall.v2z basis set is really small, accurate results are not expected. However, the minus sign for the Δ states is present, which was expected after examining the results for the perpendicular component of SrF and CaF. For the s-aug-dyall.v3z basis set, some signs are suddenly flipped, giving an even larger difference between the two Δ states and the two Π states. Because of these unexpected results, calculations using a different basis set were done, the aug-RPF-4Z basis set [45]. This is a smaller basis set than the dyall.v4z basis set, but it does include diffuse functions. The results are shown in table 33.

Table 33: Calculated perpendicular polarizability components of ground state and first five excited states of BaF in a.u. in ground state geometry, using FSCC method in combination with X2C Hamiltonian and aug-RPF-4Z basis set. There were 34 electrons included in the calculations.

State	**aug-RPF-4Z**
$X^2\Sigma$	280.37
$A^2\Delta_{3/2}$	-1565.10
$A^2\Delta_{5/2}$	1777.70
$A'^2\Pi_{1/2}$	-2870.40
$A'^2\Pi_{3/2}$	3110.70
$B^2\Sigma$	282.78

This basis set gives very similar results as the s-aug-dyall.v3z, meaning that there is probably not an error occuring from the Dyall basis sets. Unfortunately, no more time was left to investigate this issue further.

6 Discussion

In this section, some more discussion about the actual numbers of the polarizability components is given. Also, the results of the different molecules are compared, to see the impact of the atomic number of the molecule on the polarizability.

In table 34 the best obtained results for the parallel component of CaF, SrF and BaF are put next to each other (for the specifics of the calculations, see table 14, 21 and 30.)

Table 34: Best results obtained for the parallel polarizability components of ground state and first five excited states in a.u. of CaF, SrF and BaF. See table 12, 21 and 30 for the specifics of the calculations.

State	CaF	SrF	BaF
$X^2\Sigma$	96.61	123.29	170.06
$^2\Pi_{1/2}$	101.80	129.79	128.81
$^2\Pi_{3/2}$	102.50	133.62	129.52
$B^2\Sigma$	138.43	170.07	153.92
$^2\Delta_{3/2}$	47.96	62.80	66.50
$^2\Delta_{5/2}$	48.14	63.86	59.54

Something that stands out is the fact that all the Δ states have significant smaller polarizability than the other states. This can be understood by looking at the orbitals that form the molecular states. In figure 9 a schematic picture of the spatial distribution of the s-, p- and d-orbitals is shown.

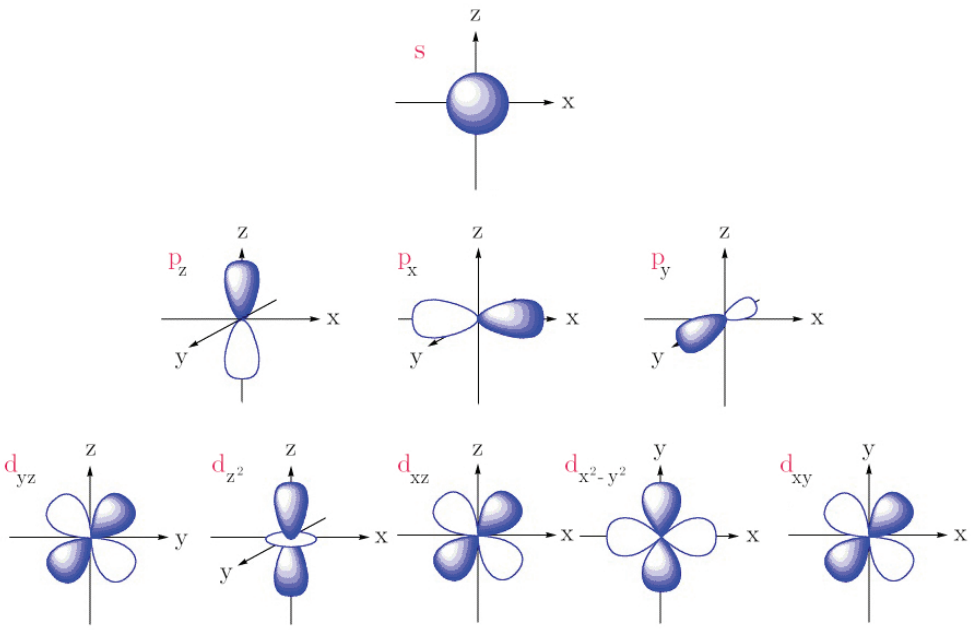

Figure 9: Schematic picture of spatial distribution of s-, p- and d-orbitals.

It turns out that the ground state of the molecules is mostly formed by a s-orbital of Ca/Sr/Ba. The

excited states are mostly formed by d- and p-orbitals of Ca/Sr/Ba. In particular, in all molecules the Δ states have the largest contribution from the d_{xy}-orbital and the $d_{x^2-y^2}$-orbital (for the orbital analysis, see the appendix). As can be seen in the figure, these orbital do not have lobes along the z-direction, in contrast to other d-orbitals. The Π states for example have contributions from the d_{xz}- and d_{yz}-orbitals, which have more charge distribution along the z-axis. Because of that, the Δ states have the smallest parallel polarizability (which was taken to be along the z-axis).

What clearly can be seen for CaF and SrF, is that for each state the polarizability increases when going from CaF to SrF. This is as expected, as SrF is a heavier molecule (CaF has 29 protons and SrF 47). As SrF has more electrons, the outer electrons in SrF are shielded more effectively from the nucleus than the outer electrons in CaF. Therefore, the outer electrons in SrF are less bound with respect to the electrons in CaF. It's therefore less difficult in SrF to pull the electrons away with an external electric field, resulting in a larger polarizability.

BaF does not follow this trend, not all polarizabilities are larger than the ones of SrF. An explanation for this can be relativistic effects due to the heavy nucleus of BaF (65 electrons). The Π states are formed mostly by d- and p-orbitals of Ba, with the largest contribution of the p-orbitals. Because of the relativistic contraction of the p-orbitals, the polarizability goes down. This compensates for the shielding effect caused by the extra electrons that BaF has with respect to SrF. Therefore, the polarizability doesn't increase as it did when going from CaF to SrF. The same argumentation can be given for the $B^2\Sigma$ state. Even though it has a large contribution from the Ba d_{z^2}-orbital, it also has large contributions from the s- and p_z-orbitals of Ba, which are relativistically contracted. The opposite is happening for the ground state of BaF, which has (next to a large Ba s-orbital contribution) a contribution from the Ba d_{z^2}-orbital. This orbital is expended due to relativistic effects, leading to a larger polarizability. For the Δ states, things are more difficult to explain. The largest contributions come from the Ba d_{xy}- and Ba $d_{x^2-y^2}$-orbitals, which will expand due to relativistic effects. However, the lobes are not directed in the z-direction, so this will not necessarily lead to an increase in parallel polarizability.

As there are no results for the perpendicular components in the correct equilibrium bond lengths for CaF and BaF, only the ones of SrF are discussed. One particular interesting thing to look at is the difference between the parallel and perpendicular component of SrF. They are shown next to each other in table 35.

Table 35: Calculated perpendicular and parallel polarizability components of ground state and first five excited states of SrF in a.u. in their own geometry. For specifics about the calculations, see table 21 and 25.

State	α_{zz}	α_{xx}
$X^2\Sigma$	123.29	192.87
$A'^2\Pi_{1/2}$	129.79	350.24
$A'^2\Pi_{3/2}$	133.62	375.05
$B^2\Sigma$	170.07	209.94
$A^2\Delta_{3/2}$	62.80	-161.05
$A^2\Delta_{5/2}$	63.86	-173.10

The ground state is formed mostly by s- and p_z-orbitals of Sr, but it also has a contribution from the Sr $d_{x^2-y^2}$-orbital. This could be the reason that the perpendicular polarizability component is somewhat larger than the parallel component. A similar argumentation can be given for the $B^2\Sigma$ state, which also has Sr $d_{x^2-y^2}$ contribution. The largest contributor to the Π states is the Sr p_x-orbital (and the Sr p_y-orbital). Therefore, the perpendicular component is a lot larger than the parallel component for the Π states. For the Δ states, the minus sign was already discussed in section 'Results'. These states are predominantly formed by $d_{x^2-y^2}$- and d_{xy}-orbitals of Sr. These orbitals both extend along the x-axis more than along the z-axis, resulting in a larger perpendicular component.

Since the results are the most complete for SrF, an error estimation can be done for the final results for the parallel and perpendicular component. A change in results is observed when using a frozen core in stead of including all electrons in the calculations. Another change occurs because of the number of diffuse functions used in the basis set.

For the parallel component, the final calculations are done with d-aug-dyall.v4z basis set and a frozen core where 34 electrons are included in the calculation. In table 36, the estimated errors in a.u. of using this frozen core and double diffuse functions is stated. These numbers are just the differences in a.u. between all electron calculations and 34 electron calculations (table 20) and d- and t-aug-dyall.v4z basis set (table 19). These differences can be added in quadrature and the last column of table 36 contains this total estimated error in percent.

Table 36: Estimated error in parallel component calculation of SrF due to the use of frozen core (34 electrons included) and d-aug-dyall.v4z basis set.

State	α_{zz}	**Estim. error (frozen core) (a.u.)**	**Estim. error (basis set) (a.u.)**	**Total estim. error (%)**
$X^2\Sigma$	123.29	-0.05	0.03	0.1
$A^2\Pi_{1/2}$	129.79	-0.06	0.89	0.7
$A^2\Pi_{3/2}$	133.62	-0.06	1.14	0.9
$B^2\Sigma$	170.07	-0.12	0.54	0.3
$B'^2\Delta_{3/2}$	62.80	0.00	-0.03	0.1
$B'^2\Delta_{5/2}$	63.86	-0.07	-0.03	0.1

For the perpendicular component, the final calculations are done with s-aug-dyall.v4z basis set and a frozen core where 16 electrons are included in the calculation. In table 37, the estimated errors in a.u. of using this frozen core and single diffuse function is stated. These numbers are the differences in a.u. between all electron calculations and 16 electron calculations (table 24) and s- and d-aug-dyall.v4z basis set (table 23).

Table 37: Estimated error in perpendicular component calculation of SrF due to the use of frozen core (16 electrons included) and s-aug-dyall.v4z basis set.

State	α_{xx}	**Estim. error (frozen core) (a.u.)**	**Estim. error (basis set) (a.u.)**	**Total estim. error (%)**
$X^2\Sigma$	192.87	-0.18	0.22	0.2
$A^2\Pi_{1/2}$	350.24	-1.87	-0.11	0.5
$A^2\Pi_{3/2}$	375.05	-2.09	-0.86	0.6
$B^2\Sigma$	209.94	0.41	8.14	3.9
$B'^2\Delta_{3/2}$	-161.05	3.29	8.73	5.8
$B'^2\Delta_{5/2}$	-173.10	3.44	-9.23	5.7

For the parallel component, the estimated errors are small compared to the error obtained between experiment and calculations for Cs (which was about 2 percent, see table 3). For the perpendicular component there are still rather large estimated errors obtained for the last three states, meaning that the use of more diffuse functions and/or smaller frozen core is preferable.

A way to improve the results even more would be to use a larger basis set (with 5 basis functions describing each orbital in stead of 4). This can be seen in figure 7 and 8, where the lines in the graphs do not end completely flat, suggesting that using a larger basis set could give different results. Also, using the four component Hamiltonian in stead of the two component X2C Hamiltonian would improve the results. For BaF, it was shown that using the X2C Hamiltonian gave a difference smaller than 0.5 percent. It is expected that for SrF this difference is even smaller, as it is a smaller system influenced less by relativistic effects.

7 Conclusion

Calculations were performed on Ba, Cs, MgH, Rb and LiH, to test the method, basis set, and Hamiltonian used. As expected, FSCC and CCSD(T) gave the best agreement with experiment for polarizability and excitation energies. The difference between the two component X2C Hamiltonian and four component Hamiltonian was smaller than 1 percent. The results improved a lot when going from small (dyall.v2z) to large (dyall.v4z) basis set. It was also shown for Cs that relativity plays a large role in heavy systems, pointing out the importance to use a relativistic approach. For the excited states of Rb it was shown that diffuse functions can be very important in the polarizability calculations, as diffuse functions give a good description of the electrons far away from the nucleus.

For the parallel components of the polarizability of CaF, SrF and BaF results are obtained for the ground and five first excited states. This was done by using the finite-field FSCC method in combination with the relativistic two component X2C Hamiltonian. The large basis set dyall.v4z was used with diffuse functions added and convergence with respect to the basis set and diffuse functions was reached. For SrF and BaF a frozen core was used, because it only gave a small difference with respect to all electron calculations.

The differences in polarizability for the three different molecules and the differences in the perpendicular and parallel component for SrF could be explained by considering the shape of the valence molecular orbitals. Also relativistic effects helped explaining some of the differences.

Because of symmetry restrictions, calculating the perpendicular component was a lot more challenging. From the results that were obtained, it showed that for all three molecules the Δ states had negative perpendicular components. This was explained using the sum-over-states polarizability description, where mixing of states could result in negative polarizabilities for excited states.

For BaF some unexpected results were obtained when using the s-aug-dyall.v3z basis set. When using the different aug-RPF-4Z basis set, similar results were obtained. This matter wasn't investigated further, due to a lack of time. For SrF, calculations were done in the proper geometry for each state. However, due to computational reasons some of the accuracy was compensated by using a frozen core and only adding one diffuse function to the basis set. Also for CaF the perpendicular calculations took really long, leaving no time to do calculations in the proper geometries of the states. An estimate of the difference between s-aug-dyall.v3z and s-aug-dyall.v4z basis set, as well as all electron and frozen core calculations was done.

In order to obtain convergence with respect to basis set and diffuse functions for the perpendicular components, more computational resources would be needed.

References

[1] L. D. Carr, D. DeMille, R. V. Krems, and J. Ye. Cold and ultracold molecules: science, technology and applications. *New J. Phys.*, **11**:055049, 2009.

[2] M. S. Safronova, U. I. Safronova, and Charles W. Clark. Magic wavelengths for optical cooling and trapping of potassium. *Phys. Rev. A*, **87**:052504, 2013.

[3] L. Anderegg, B. L. Augenbraun, Y. Bao, S. Burchesky, L. W. Cheuk, W. Ketterle, and J. M. Doyle. Laser Cooling of Optically Trapped Molecules. *Nature Physics*, DOI: https://doi.org/10.1038/s41567-018-0191-z, June 2018.

[4] J. J. Hudson, D. M. Kara, I. J. Smallman, B. E. Sauer, M. R. Tarbutt, and E. A. Hinds. Improved measurement of the shape of the electron. *Nature*, **473**:493–496, 2011.

[5] D. M. Kara, I. J. Smallman, J. J. Hudsonand B. E. Sauer, M. R. Tarbutt, and E. A. Hinds. Measurement of the electron's electric dipole moment using YbF molecules: methods and data analysis. *New Journal of Physics*, **14**:103051, 2012.

[6] S. M. Barr and A. Zee. Electric Dipole Moment of the Electron and of the Neutron. *Phys. Rev. Lett.*, **65**:21, 1990.

[7] NL–eEDM collaboration. Measuring the electric dipole moment of the electron in BaF. arXiv:1804.10012 [physics.atom-ph].

[8] V.S. Prasannaa, A.C. Vutha, M. Abe, and B.P. Das. Mercury Monohalides: Suitability for Electron Electric Dipole Moment Searches. *Phys. Rev. Lett*, **114**:183001, 2015.

[9] A. A. K. Mohammed and B. Champagne P. A. Limacher. Finding optimal finite field strengths allowing for a maximum of precision in the calculation of polarizabilities and hyperpolarizabilities. *Journal of Computational Chemistry*, **34:17**:1497–1507, 2013.

[10] C. D. Sherrill. *A Brief Review of Elementary Quantum Chemistry: The Born-Oppenheimer Approximation.* http://vergil.chemistry.gatech.edu/notes/quantrev/node31.html, (accessed: 14-05-2018).

[11] K. B. Yatsimirskii. Relativistic effects in chemistry. *Theoretical and Experimental Chemistry*, **31:3**, 1995.

[12] E. Eliav and U. Kaldor. Energies and Other Properties of Heavy Atoms and Molecules. *Quantum Systems in Chemistry and Physics*, **1**:161–176, 2000.

[13] T. Saue. Relativistic hamiltonians for chemistry: a primer. *Chem. Phys. Chem.*, **12**:3077–3094, 2011.

[14] Dirac Program. *X2C and local X2C.* http://www.diracprogram.org/doc/master/tutorials /two_component_hamiltonians/x2c_mol_loc.html, (accessed: 09-07-2018).

[15] C. D. Sherrill. *An Introduction to Hartree-Fock Molecular Orbital Theory.* http://vergil.chemistry.gatech.edu/notes/hf-intro/hf-intro.pdf, (accessed: 12-07-2018).

[16] D. K. Griffiths. *Introduction to Quantum Mechanics*. New Jersey. Upper Saddle River, 1995.

[17] R. F. Bishop. The Coupled-Cluster Method. *Phys. Tod.*, **50**:52–60, 1987.

[18] P. J. Knowles, C. Hampel, and H. J. Werner. Coupled cluster theory for high spin, open shell reference wave functions. *The Journal of Chemical Physics*, **99**:5219, 1993.

[19] A. S. P. Gomes and C. R. Jacob. Quantum-chemical embedding methods for treating local electronic excitations in complex chemical systems. *Annu. Rep. Prog. Chem., Sect. C: Phys. Chem.*, **108**:222–277, 2012.

[20] M. Dolg. *Computational Methods in Lanthanide and Actinide Chemistry*. West Sussex. John Wiley Sons, Ltd, 2015.

[21] I. Lindgren and J. Morrison. *Atomic Many-Body Theory*. New York. Springer-Verlag Berlin Heidelberg, 1982.

[22] I. Lindgren and D. Mukherjee. On the connectivity criteria in the open-shell coupled-cluster theory for general model spaces. *Physics Reports*, **151:2**:93–127, 1987.

[23] A. Borschevsky. http://www.tau.ac.il/∼ ephraim/Appendix_1.pdf, (accessed: 15-02-2018).

[24] K.G. Dyall. http://dirac.chem.sdu.dk. *Chem. Phys. Chem. A.*, **113**:12638, 2009.

[25] R. Bast, T. Saue, L. Visscher, and H. J. Aa. Jensen. *DIRAC program*. http://www.diracprogram.org, (2017).

[26] P.J. Linstrom and W.G. Mallard. NIST Chemistry WebBook, NIST Standard Reference Database Number 69. *National Institute of Standards and Technology, Gaithersburg MD*, **20899**:doi:10.18434/T4D303, retrieved July, 2018.

[27] M. D. Gregoire and I. Hromada. Measurements of the ground-state polarizabilities of Cs, Rb, and K using atom interferometry. *Phys. Rev. A*, **92**:052513, 2015.

[28] A. Serrano and S. Canuto. Calculated polarizabilities and gradients: Rayleigh and Raman scattering activities for the MgH molecule. *Journal of Molecular Structure (Theochem)*, **432**:69–74, 1998.

[29] A.D. McLean and G.S. Chandler. Contracted Gaussian basis sets for molecular calculations. I. Second row atoms, Z=11–18. *J. Chem. Phys.*, **72**:5639, 1980.

[30] P. Siegbahn and B. Lui. An accurate three-dimensional potential energy surface for H3. *J. Chem. Phys.*, **68**:2457, 1978.

[31] C. Zhu, A. Dalgarno, S. G. Porsev, and A. Derevianko. Dipole polarizabilities of excited alkali-metal atoms and long-range interactions of ground- and excited-state alkali-metal atoms with helium atoms. *Phys. Rev. A*, **70**:032722–1 – 032722–5, 2004.

[32] R. W. Molof, H. L. Schwartz, T. M. Miller, and B. Bederson. Measurements of electric dipole polarizabilities of the alkali-metal atoms and the metastable noble-gas atoms. *Phys. Rev. A*, **10**:1131, 1974.

[33] C. Yamada and E. J. Hirota. Infrared diode laser spectroscopy of lithium hydride. *J. Chem. Phys.*, **88**:6702, 1988.

[34] M. Mérawa, D. Bégué, and A. Dargelos. Ab Initio Calculation of the Polarizability for the Ground State X1+ and the First Low-Lying Excited States a3+ and A1+ of LiH and NaH. *J. Phys. Chem. A*, **107**:9628–9633, 2003.

[35] G. H. Jeung. Inclusion of core-valence correlation effects in pseudopotential calculations. II. K_2 and KH lowest Σ^+ potential curves from valence-correlated wavefunctions. *J. Phys. B: At. Mol. Phys.*, **16**:699, 1983.

[36] F. H. Crawford and Jr. T. Jorgensen. The band spectra of the hydrides of lithium. *Phys. Rev.*, **47**:932, 1935.

[37] Y. Hao, M. Ilias, E. Eliav, P. Schwerdtfeger, V. V. Flambaum, and A. Borschevsky. The nuclear anapole moment interaction in BaF from relativistic coupled cluster theory. arXiv:1808.02771 [physics.atom-ph].

[38] J. Verges *et al.* The B' $^2\Delta$ state of CaF. *J. Phys. B: At. Mol. Opt. Phys.*, **26**:279, 1993.

[39] F. C. Grozema, R. Telesca, H. T. Jonkman, L. D. A. Siebbeles, and J. G. Snijders. Excited state polarizabilities of conjugated molecules calculated using time dependent density functional theory. *J. Chem. Phys.*, **115**:21, 2001.

[40] Jr. C. A. Fowler. New Absorption Spectra of the Alkaline Earth Fluorides. *Phys. Rev.*, **59**:645, 1941.

[41] M. B. Kosicki, D. Kedziera, and P. S. Żuchowski. Ab Initio Study of Chemical Reactions of Cold SrF and CaF Molecules with Alkali-Metal and Alkaline-Earth-Metal Atoms: The Implications for Sympathetic Cooling. *J. Phys. Chem. A*, **121**:41524159, 2017.

[42] E. R. Meyer and J. L. Bohn. Chemical pathways in ultracold reactions of SrF molecules. *Phys. Rev. A*, **83**:032714, 2011.

[43] R.F. Barrow *et al.* The metastable A' $^2\Delta$ state of BaF . *Chem. Phys. Lett.*, **147**:6, 1988.

[44] K. P. Huber and G. Herzberg. *Constants of diatomic molecules.* New York. Van Nostrand Reinhold, 1979.

[45] T. Q. Teodoro, A. B. F. da Silva, and R. L. A. Haiduke. Relativistic Prolapse-Free Gaussian Basis Set of Quadruple-ζ Quality: (aug-)RPF-4Z. I. The s- and p-Block Elements. *J. Chem. Theory Comput.*, **10(9)**:3800–3806, 2014.

8 Appendix

The orbital analysis obtained from the Dirac-Hartree-Fock calculations is shown here. Only the analysis of BaF is shown, as the ones for SrF and CaF are very similar. Also only one picture of the $^2\Pi$ and $^2\Delta$ states is shown, as they are as well very similar. The pictures are from calculations using the d-aug-dyall.v4z basis set and zero external electric field. The largest contributions are highlighted.

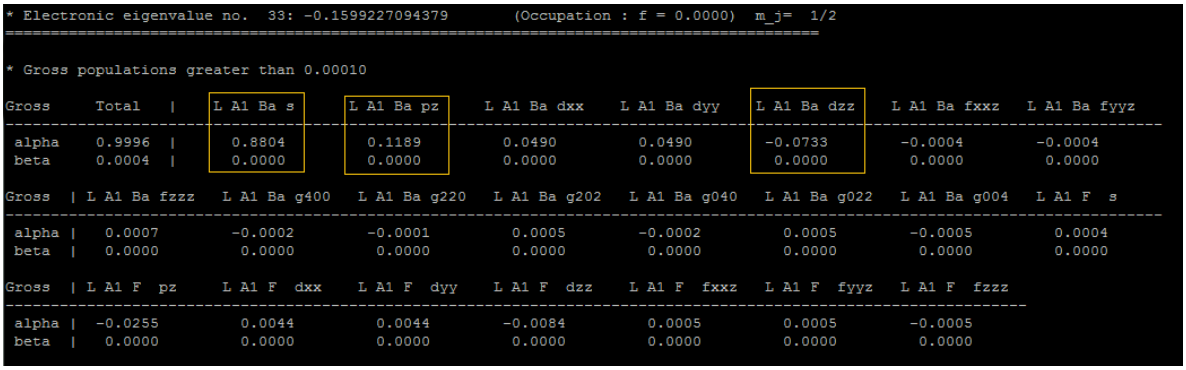

* Electronic eigenvalue no. 33: -0.1599227094379 (Occupation : f = 0.0000) m_j= 1/2

* Gross populations greater than 0.00010

Gross	Total	L A1 Ba s	L A1 Ba pz	L A1 Ba dxx	L A1 Ba dyy	L A1 Ba dzz	L A1 Ba fxxz	L A1 Ba fyyz
alpha	0.9996	0.8804	0.1189	0.0490	0.0490	-0.0733	-0.0004	-0.0004
beta	0.0004	0.0000	0.0000	0.0000	0.0000	0.0000	0.0000	0.0000

Gross	L A1 Ba fzzz	L A1 Ba g400	L A1 Ba g220	L A1 Ba g202	L A1 Ba g040	L A1 Ba g022	L A1 Ba g004	L A1 F s
alpha	0.0007	-0.0002	-0.0001	0.0005	-0.0002	0.0005	-0.0005	0.0004
beta	0.0000	0.0000	0.0000	0.0000	0.0000	0.0000	0.0000	0.0000

Gross	L A1 F pz	L A1 F dxx	L A1 F dyy	L A1 F dzz	L A1 F fxxz	L A1 F fyyz	L A1 F fzzz
alpha	-0.0255	0.0044	0.0044	-0.0084	0.0005	0.0005	-0.0005
beta	0.0000	0.0000	0.0000	0.0000	0.0000	0.0000	0.0000

Figure 10: Ground state $^2\Sigma$ orbital analysis of BaF.

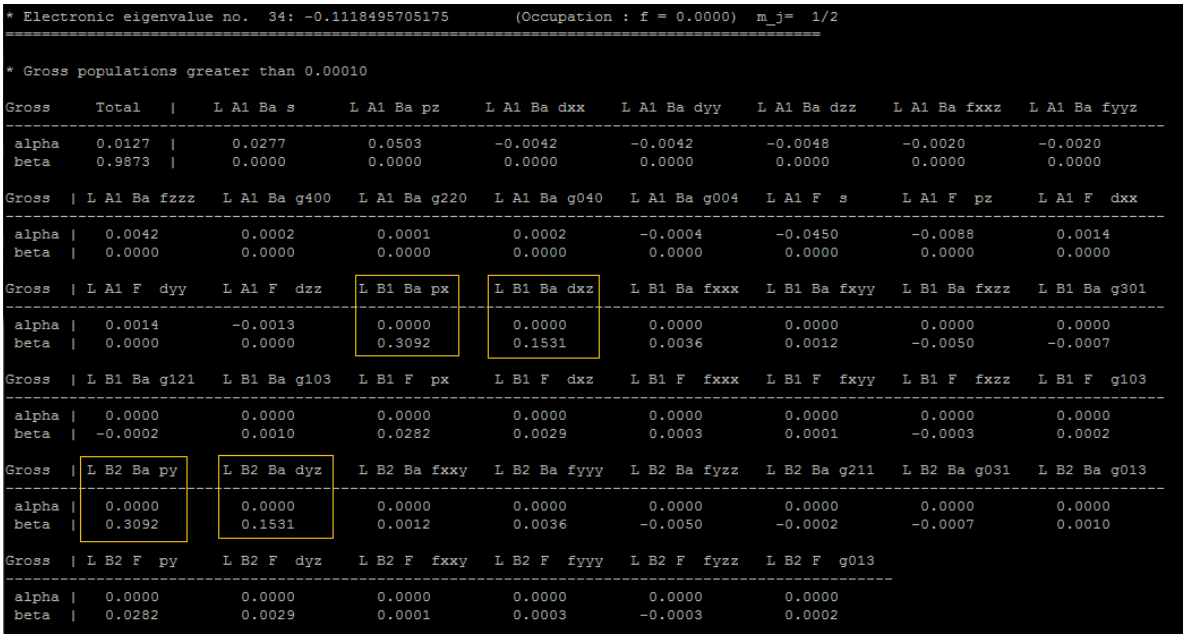

* Electronic eigenvalue no. 34: -0.1118495705175 (Occupation : f = 0.0000) m_j= 1/2

* Gross populations greater than 0.00010

Gross	Total	L A1 Ba s	L A1 Ba pz	L A1 Ba dxx	L A1 Ba dyy	L A1 Ba dzz	L A1 Ba fxxz	L A1 Ba fyyz
alpha	0.0127	0.0277	0.0503	-0.0042	-0.0042	-0.0048	-0.0020	-0.0020
beta	0.9873	0.0000	0.0000	0.0000	0.0000	0.0000	0.0000	0.0000

Gross	L A1 Ba fzzz	L A1 Ba g400	L A1 Ba g220	L A1 Ba g040	L A1 Ba g004	L A1 F s	L A1 F pz	L A1 F dxx
alpha	0.0042	0.0002	0.0001	0.0002	-0.0004	-0.0450	-0.0088	0.0014
beta	0.0000	0.0000	0.0000	0.0000	0.0000	0.0000	0.0000	0.0000

Gross	L A1 F dyy	L A1 F dzz	L B1 Ba px	L B1 Ba dxz	L B1 Ba fxxx	L B1 Ba fxyy	L B1 Ba fxzz	L B1 Ba g301
alpha	0.0014	-0.0013	0.0000	0.0000	0.0000	0.0000	0.0000	0.0000
beta	0.0000	0.0000	0.3092	0.1531	0.0036	0.0012	-0.0050	-0.0007

Gross	L B1 Ba g121	L B1 Ba g103	L B1 F px	L B1 F dxz	L B1 F fxxx	L B1 F fxyy	L B1 F fxzz	L B1 F g103
alpha	0.0000	0.0000	0.0000	0.0000	0.0000	0.0000	0.0000	0.0000
beta	-0.0002	0.0010	0.0282	0.0029	0.0003	0.0001	-0.0003	0.0002

Gross	L B2 Ba py	L B2 Ba dyz	L B2 Ba fxxy	L B2 Ba fyyy	L B2 Ba fyzz	L B2 Ba g211	L B2 Ba g031	L B2 Ba g013
alpha	0.0000	0.0000	0.0000	0.0000	0.0000	0.0000	0.0000	0.0000
beta	0.3092	0.1531	0.0012	0.0036	-0.0050	-0.0002	-0.0007	0.0010

Gross	L B2 F py	L B2 F dyz	L B2 F fxxy	L B2 F fyyy	L B2 F fyzz	L B2 F g013
alpha	0.0000	0.0000	0.0000	0.0000	0.0000	0.0000
beta	0.0282	0.0029	0.0001	0.0003	-0.0003	0.0002

Figure 11: Excited state $^2\Pi_{1/2}$ orbital analysis of BaF.

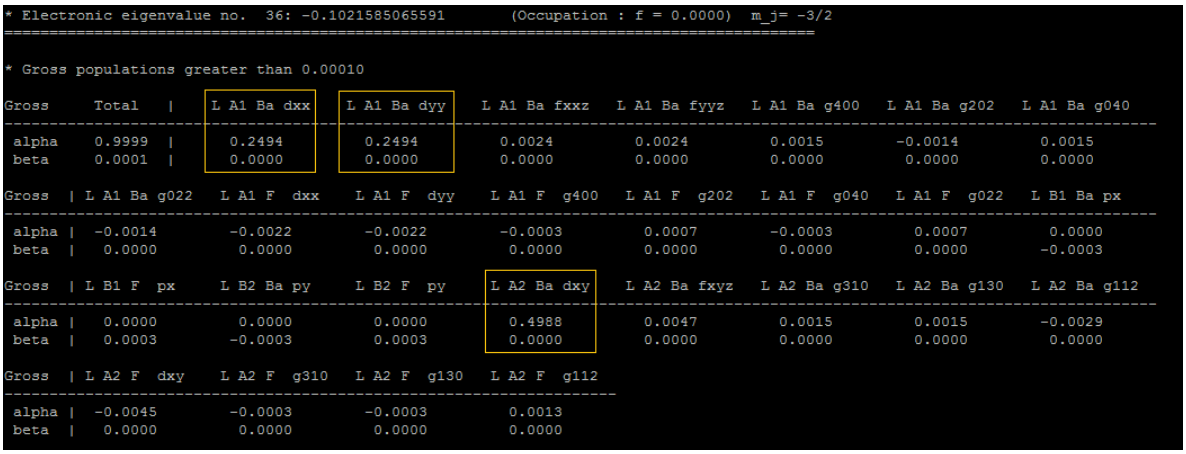

```
* Electronic eigenvalue no.  36: -0.1021585065591       (Occupation : f = 0.0000)  m_j= -3/2
================================================================================

* Gross populations greater than 0.00010

Gross     Total   |   L A1 Ba dxx   L A1 Ba dyy   L A1 Ba fxxz   L A1 Ba fyyz   L A1 Ba g400   L A1 Ba g202   L A1 Ba g040
-------------------------------------------------------------------------------------------------------------------------
 alpha    0.9999  |     0.2494        0.2494        0.0024         0.0024         0.0015        -0.0014         0.0015
 beta     0.0001  |     0.0000        0.0000        0.0000         0.0000         0.0000         0.0000         0.0000

Gross  | L A1 Ba g022   L A1 F  dxx    L A1 F  dyy    L A1 F  g400   L A1 F  g202   L A1 F  g040   L A1 F  g022   L B1 Ba px
-------------------------------------------------------------------------------------------------------------------------
 alpha |  -0.0014        -0.0022        -0.0022        -0.0003         0.0007        -0.0003         0.0007         0.0000
 beta  |   0.0000         0.0000         0.0000         0.0000         0.0000         0.0000         0.0000        -0.0003

Gross  | L B1 F  px     L B2 Ba py     L B2 F  py     L A2 Ba dxy    L A2 Ba fxyz   L A2 Ba g310   L A2 Ba g130   L A2 Ba g112
-------------------------------------------------------------------------------------------------------------------------
 alpha |   0.0000         0.0000         0.0000         0.4988         0.0047         0.0015         0.0015        -0.0029
 beta  |   0.0003        -0.0003         0.0003         0.0000         0.0000         0.0000         0.0000         0.0000

Gross  | L A2 F  dxy    L A2 F  g310   L A2 F  g130   L A2 F  g112
-------------------------------------------------------------------
 alpha |  -0.0045        -0.0003        -0.0003         0.0013
 beta  |   0.0000         0.0000         0.0000         0.0000
```

Figure 12: Excited state $^2\Delta_{3/2}$ orbital analysis of BaF.

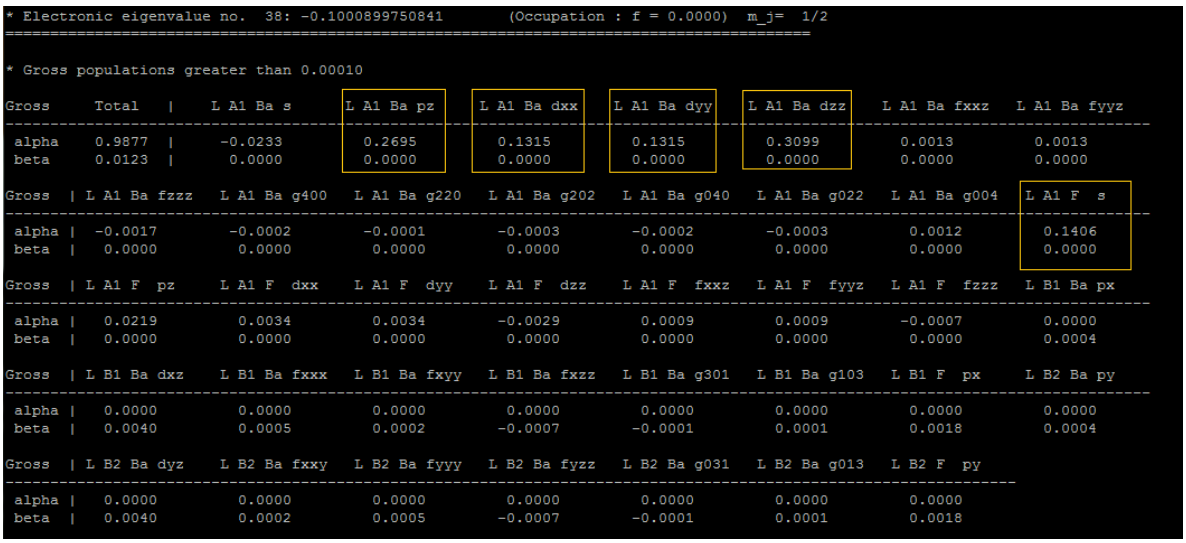

```
* Electronic eigenvalue no.  38: -0.1000899750841       (Occupation : f = 0.0000)  m_j=  1/2
================================================================================

* Gross populations greater than 0.00010

Gross     Total   |    L A1 Ba s     L A1 Ba pz     L A1 Ba dxx    L A1 Ba dyy    L A1 Ba dzz    L A1 Ba fxxz   L A1 Ba fyyz
-------------------------------------------------------------------------------------------------------------------------
 alpha    0.9877  |     -0.0233         0.2695         0.1315         0.1315         0.3099         0.0013         0.0013
 beta     0.0123  |      0.0000         0.0000         0.0000         0.0000         0.0000         0.0000         0.0000

Gross  | L A1 Ba fzzz   L A1 Ba g400   L A1 Ba g220   L A1 Ba g202   L A1 Ba g040   L A1 Ba g022   L A1 Ba g004   L A1 F  s
-------------------------------------------------------------------------------------------------------------------------
 alpha |  -0.0017        -0.0002        -0.0001        -0.0003        -0.0002        -0.0003         0.0012         0.1406
 beta  |   0.0000         0.0000         0.0000         0.0000         0.0000         0.0000         0.0000         0.0000

Gross  | L A1 F  pz     L A1 F  dxx    L A1 F  dyy    L A1 F  dzz    L A1 F  fxxz   L A1 F  fyyz   L A1 F  fzzz   L B1 Ba px
-------------------------------------------------------------------------------------------------------------------------
 alpha |   0.0219         0.0034         0.0034        -0.0029         0.0009         0.0009        -0.0007         0.0000
 beta  |   0.0000         0.0000         0.0000         0.0000         0.0000         0.0000         0.0000         0.0004

Gross  | L B1 Ba dxz    L B1 Ba fxxx   L B1 Ba fxyy   L B1 Ba fxzz   L B1 Ba g301   L B1 Ba g103   L B1 F  px     L B2 Ba py
-------------------------------------------------------------------------------------------------------------------------
 alpha |   0.0000         0.0000         0.0000         0.0000         0.0000         0.0000         0.0000         0.0000
 beta  |   0.0040         0.0005         0.0002        -0.0007        -0.0001         0.0001         0.0018         0.0004

Gross  | L B2 Ba dyz    L B2 Ba fxxy   L B2 Ba fyyy   L B2 Ba fyzz   L B2 Ba g031   L B2 Ba g013   L B2 F  py
-------------------------------------------------------------------------------------------------------------
 alpha |   0.0000         0.0000         0.0000         0.0000         0.0000         0.0000         0.0000
 beta  |   0.0040         0.0002         0.0005        -0.0007        -0.0001         0.0001         0.0018
```

Figure 13: Excited state $^2\Sigma$ orbital analysis of BaF.